Journal of Materials Chemistry B

ROYAL SOCIETY OF CHEMISTRY

REVIEW

View Article Online
View Journal | View Issue

Cite this: J. Mater. Chem. B, 2025, 13, 1599

Advances in nanozymes with peroxidase-like activity for biosensing and disease therapy applications

Xiaohua Yuan,[ab] Xun He,[c] Jiwen Fan,[ab] Yunze Tai,[ab] Yongchao Yao,[ab] Yao Luo,[ab] Jie Chen,[ab] Han Luo,[ab] Xingli Zhou,[c] Fengming Luo,[cd] Qian Niu,*[ab] Wenchuang (Walter) Hu,*[ab] Xuping Sun*[ce] and Binwu Ying*[ab]

Received 14th October 2024,
Accepted 9th December 2024

DOI: 10.1039/d4tb02315c

rsc.li/materials-b

Natural enzymes are crucial in biological systems and widely used in biomedicine, but their disadvantages, such as insufficient stability and high cost, have limited their widespread application. Since discovering the enzyme-like activity of Fe_3O_4 nanoparticles, extensive research progress in diverse nanozymes has been made with their in-depth investigation, resulting in rapid development of related nanotechnologies. Nanozymes can compensate for the defects of natural enzymes and show higher stability with lower costs. Among them, peroxidase (POD)-like nanozymes have attracted extensive attention in biomedical applications owing to their efficient catalytic performance and diverse structures. This review explores different types of nanozymes with POD-like activity and discusses their activity regulation, particularly emphasizing their latest development trends and advances in biosensing and disease treatment. Finally, the challenges and prospects for the development of POD-like nanozymes and their potential future applications in the biomedical field are also provided.

1. Introduction

Natural enzymes are powerful biocatalysts that are used to selectively and efficiently catalyze various biochemical reactions. Natural enzymes have high selectivity and efficient catalytic activity and play an important role in many fields, such as food industry, disease diagnosis and treatment, and environmental monitoring.[1] POD is a natural enzyme that enables the conversion of H_2O_2 into H_2O, during which the substrate is oxidized to its corresponding oxide. Horseradish peroxidase (HRP), as a typical peroxidase, has been studied over the years as a useful tool to catalyze H_2O_2. However, disadvantages such as low operational stability, high cost, difficult storage, easy inactivation, cumbersome and time-consuming preparation have hindered its widespread application.[2] Therefore, the development of new artificial enzymes to replace POD is of great significance to broaden their applications in biology.

In recent years, various nanomaterials have exhibited excellent catalytic activity by mimicking the function or structure of peroxidase, such as metal/gold composite nanoparticles, carbon-based nanomaterials, metal–organic frameworks (MOFs), and single-atom nanozymes (SAzymes). Because at least one of the three dimensions of nanomaterials is in the nanoscale range, their small size endows them with many specific effects such as small size effect, surface effect and quantum size effect, compared with other materials. In addition, nanomaterials have the advantages of flexible structural design and composition, as well as high active sites, which can enhance their catalytic activity. Since Yan *et al.* discovered that Fe_3O_4 magnetic nanoparticles have POD-like properties, they have been widely used in many fields, such as the separation and capture of analytes, sensing, and treatment.[3]

POD-like nanozymes are dual-substrate nanozymes, which can catalyze the hydrogen acceptor to produce a large number of oxidative free radicals in the presence of the first substrate, which is a hydrogen acceptor (such as H_2O_2), and then rapidly oxidize the hydrogen donor, which is the second substrate. Depending on the hydrogen donor, POD-like nanozymes can mimic the activities of various enzymes, such as peroxidase, glutathione (GSH) peroxidase, and lipid peroxidase. There are various hydrogen receptors for peroxidases. For example, the hydrogen acceptor for HRP is H_2O_2, and the hydrogen acceptor

[a] Department of Laboratory Medicine/Clinical Laboratory Medicine Research Center, West China Hospital, Sichuan University, Chengdu 610041, Sichuan, China. E-mail: yingbinwu@scu.edu.cn, huwenchuang@wchscu.cn, niuqian991@scu.edu.cn
[b] Frontiers Science Center for Disease-related Molecular Network, West China Hospital, Sichuan University, Chengdu 610041, Sichuan, China
[c] Center for High Altitude Medicine, West China Hospital, Sichuan University, Chengdu 610041, Sichuan, China. E-mail: sunxp@wchscu.edu.cn
[d] Department of Pulmonary and Critical Care Medicine, West China Hospital, Sichuan University, Chengdu 610041, Sichuan, China
[e] College of Chemistry, Chemical Engineering and Materials Science, Shandong Normal University, Jinan 250014, Shandong, China

for lipid peroxidase is lipid peroxide. The free radicals catalyzed by hydrogen acceptors can oxidize various hydrogen donor substrates, including small-molecule metabolites (formic acid, methanol, ethanol, *etc.*) and biological macromolecules (nucleic acids, proteins, polysaccharides, lipids, *etc.*). Taking the earliest horseradish POD-like nanozyme as an example, its activity detection method typically employs the same approach as that used for natural HRP.[4] When the reaction is catalyzed by the POD-like nanozyme using H_2O_2 as the hydrogen acceptor, numerous intermediate $^{\bullet}OH$ radicals are generated, which then oxidize hydrogen donors. In particular, the catalytic pathway of POD-like nanozyme mainly involves reactive oxygen species (ROS) formation and electron transfer. For ROS production, the nanozyme reacts with H_2O_2 to produce ROS ($^{\bullet}OH$, $O^{2-\bullet}$, $HO_2^{\bullet}$, *etc.*), which is responsible for further oxidation. Fe_3O_4 NPs are the first proposed nanozymes with intrinsic POD-like activity, in which the surface Fe^{2+} plays a leading role in activating H_2O_2 and producing ROS *via* the Fenton or Haber–Weiss reaction.[5] For the electron transfer process, the substrate is first adsorbed onto the surface of the nanozyme, providing electrons. Large specific surface areas with abundant active sites or variable oxidation states confer the nanozyme with increased electron density and excellent mobility, resulting in redox reactions between the substrate and H_2O_2. Rapid electron transfer from the substrate to H_2O_2 further accelerates substrate oxidation and H_2O_2 reduction.[6]

While some reviews have been published on POD-like nanomaterials, it is worth noting that some of them have a narrow focus, discussing only a specific type of POD-like nanozyme or highlighting a limited range of biomedical applications. Based on this consideration, this article will provide a comprehensive review of POD-like nanomaterials and their biomedical applications (Fig. 1). First, we briefly introduce different types of nanozymes with POD-like activity. Then, strategies for endowing POD-like activity to nanozymes are summarized. Furthermore, the recent research progress of POD-like nanozymes in the field of biosensing and disease treatment is comprehensively reviewed. Finally, our insights into the prospects and challenges of the development of POD-like nanozymes are presented. The aim is to provide valuable and comprehensive information to scientists in the fields of materials science and biomedical research, and promote the development of interdisciplinary fields.

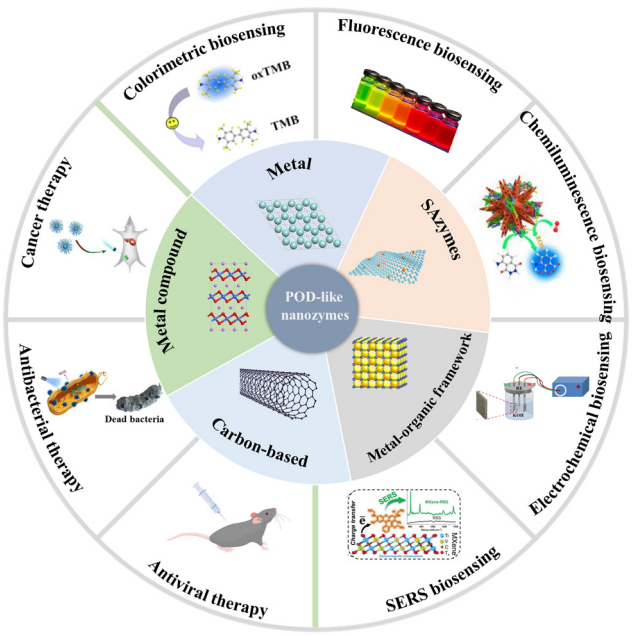

Fig. 1 Overview of POD-like nanozymes for biomedical applications.

2. Classification of POD-like nanozymes

The simulated enzyme activity of nanomaterials is generally believed to be produced by the atoms on the surface and in the core of the material. Although it has been widely reported that size, morphology, surface modification, pH, and temperature affect the nanozyme activity, the elemental composition is still the kernel factor that determines the catalytic activity of the nanozyme. It has been reported that more than 40 elements and about 100 different types of nanozymes have been discovered. Its classification can be made from different angles. Based on material types, they are mainly classified into the following categories. Table 1 summarizes the synthesis, structure, and applications of various POD-like nanozymes.

2.1. Metal nanozymes

Metal nanomaterials such as gold (Au), silver (Ag), iridium (Ir), palladium (Pd), platinum (Pt), ruthenium (Ru), copper (Cu) and lanthanides have been reported to have enzyme-like catalytic activity. The main synthesis methods include the general reduction method,[22] the co-reduction method,[23] and the displacement reaction method.[24] Metal nanozymes exhibit POD-like nanozyme activities, facilitating their incorporation into diverse research domains encompassing chemical analysis, biological sensing, antimicrobial strategies, and disease treatment methodologies.[25] Furthermore, these metal-based nanomaterials boost remarkable versatility, allowing for facile modification with chemical functionalities such as $–NH_2$, –COOH, and –SH. Their ease of conjugation to biomolecules such as antibodies, enzymes, and oligonucleotides underscores their immense potential in the development of advanced biosensing platforms.[26] In addition, advances in the field have seen the emergence of bimetallic and even trimetallic nanozymes, including Pt–Ir nanocubes and Pt–Pd hybrid nanozymes, which have attracted considerable attention and have been extensively reported for their unique properties and potential applications. Compared with single-metal nanozymes, bimetal or trimetal nanozymes tend to exhibit higher stability and catalytic activity due to the synergistic catalytic effect, so they have potential applications in the field of biosensing and therapy.[27,28] For example, Fu *et al.* prepared a porous Au@Pt nanoparticle with ultra-high POD-like activity using a seed-mediated growth method that enables colorimetric detection of the SARS-CoV2 spike protein.[29] Li *et al.* ingeniously developed a Ag/Pd bimetallic nanozyme that exhibits

Table 1 Different types of POD-like nanozymes

	Nanozyme	Preparation method	Structure	Application	Ref.
Metal nanozymes	GNPs	General reduction method	Nanoparticles	The structure–activity relationship of catalytic properties of nanozyme was studied	7
	Au/Pt NPs	Coreduction method	Nanoparticles	Au/Pt alloy nanoshells with different catalytic properties were prepared	8
	Au/Pt NPs	Electrodeposition method	Nanoparticles	The size and morphology of nanozymes were controlled by controlling electrodeposition parameters	9
	Ag/Au NPs	Replacement reaction method	Core–shell	The solvent and temperature determine the structure and composition of the nanoparticles formed by the displacement reaction	10
	Pd Nanocrystals	Solvothermal method	Either cubic or octahedral shapes	To investigate the relationship between the catalytic activity of Pd nanozyme and the exposed crystal surface	11
Metal compound nanozymes	Fe_3O_4 NPs	Solvothermal ion-exchange methods	Nanosphere	To prepare different types of iron oxide nanozymes	12
	Fe_3O_4@TiO_2/TP	Solvothermal and ion-exchange methods	Nanoparticle	preparation of efficient catalysts	13
	GO NPs	Hummers' method and ultrasonic stripping method	Clustered layer	To prepare nanomaterials with POD-like activity for the determination of heavy metal ions	14
	Fe_3C@FeN-CM	Hydrothermal method and high temperature calcination method	Polyhedral structure	Multi-enzyme activity and rapid detection of food quality and safety	15
	IO-MC	Impregnation method and high-temperature calcination method	Rod-like morphology	With POD-like activity, they realize highly sensitive detection of glucose	16
Carbon-based nanozymes	N-Doped Carbon Sheets	High temperature pyrolytic cracking	Sheet structure	For the determination of hydrogen peroxide, glucose and ascorbic acid	17
Metal–organic framework nanozymes	MOF-818	Direct synthesis technique	Octahedron in shape	Specific catechol oxidase activity	18
	AuPt/MOF	Post-synthetic modification	sheets structure	A new metal ionizer or ligand is introduced into MOFs to give them enzyme-like catalytic activity	19
	ZIF8	Composite preparation method	Rhombic dodecahedral	MOFs act as carriers to support other nanozymes	20
Single-atom Nanozymes	FeN_5 SA/CNF	Spatial constraint synthesis strategy	Mesoporous	The active site of Fe–N_5 is similar to the active site of cytochrome P450 and has good oxidase-like activity	21

intrinsic POD-like activity,[30] efficiently decomposing H_2O_2 into hydroxyl radicals ($^{\bullet}OH$). By harnessing the synergistic interplay of this enzymatic property with its intrinsic photothermal effects, the nanozyme achieves remarkable enhancement in its antitumor capabilities (Fig. 2a–c). Furthermore, based on ultra-small Ir/Ru alloy nanoparticles, Wei *et al.* designed a multi-enzyme active therapeutic platform with tumor microenvironment-responsive properties and achieved synergies between tumor starvation therapy and catalytic therapy by additionally loading glucose oxidase.[31] Besides the synergistic effect of Au NPs and other materials, the fabricated nanozyme exhibits enhanced POD-like activity, making it a potential alternative to peroxidase. Chen *et al.* designed a hybrid nanozyme, gold nanoparticles/N-doped porous carbon (Au NPs/NPC), which is fabricated *via* a supramolecular assembly-assisted pyrolysis strategy and engineered as a peroxidase mimic.[32] It exhibits broad prospects in biosensing by mimicking enzymes in catalytic fields and thus helping in clinical diagnosis.

2.2. Metal compound nanozymes

Metal compound nanozymes mainly include metal oxide nanozymes, metal sulfide nanozymes, metal selenide nanozymes, and metal phosphide nanozymes, and the main synthesis methods include solvothermal method, liquid-phase precipitation method, and thermal decomposition method. Metal oxides are the most studied and applied nanozymes. Among them, Fe_3O_4 is the most desired by researchers. Its activity was first reported in 2007.[38,39] Fe_3O_4 exhibits similar catalytic kinetics to natural HRP in the enzyme-like catalytic process, and kinetic studies show that the reaction process of Fe_3O_4 follows the ping-pong catalytic mechanism. That is, Fe_3O_4 first reacts with H_2O_2 to form $^{\bullet}OH$, and $^{\bullet}OH$ combines with Fe_3O_4 to form a complex, which further interacts with the reducing substrate to catalyze the oxidation of the substrate, and finally, Fe_3O_4 returns to its initial state. In 2011, the Tremel group reported that V_2O_5 has POD-like activity, just like Fe_3O_4. They found that V_2O_5 works best at a pH of 4.0. When tested in kinetic experiments using Michaelis–Menten principles and ABTS (2,2′-azino-bis(3-ethylbenzothiazoline-6-sulfonic acid)) as the substrate, V_2O_5 exhibited a similar catalytic behavior to natural vanadium-dependent haloperoxidase. Moreover, the catalytic mechanism of V_2O_5 follows the ping-pong mechanism (Fig. 2d).

Metal sulfides, including MoS, CuS, and FeS, can also be used as peroxidase mimics. Xu *et al.* used a solvothermal method to convert garlic-derived organosulfur compounds. Compared with organic sulfides, the antimicrobial efficiency of nano-iron sulfides is more than 500-fold higher when acting on pathogenic and drug-resistant bacteria, and the mechanism suggests that the POD-like activity of nano-iron sulfides can accelerate the release of polysulfides, thereby effectively enhancing antimicrobial activity.[40] In addition, bimetallic sulfides exhibit good POD-like

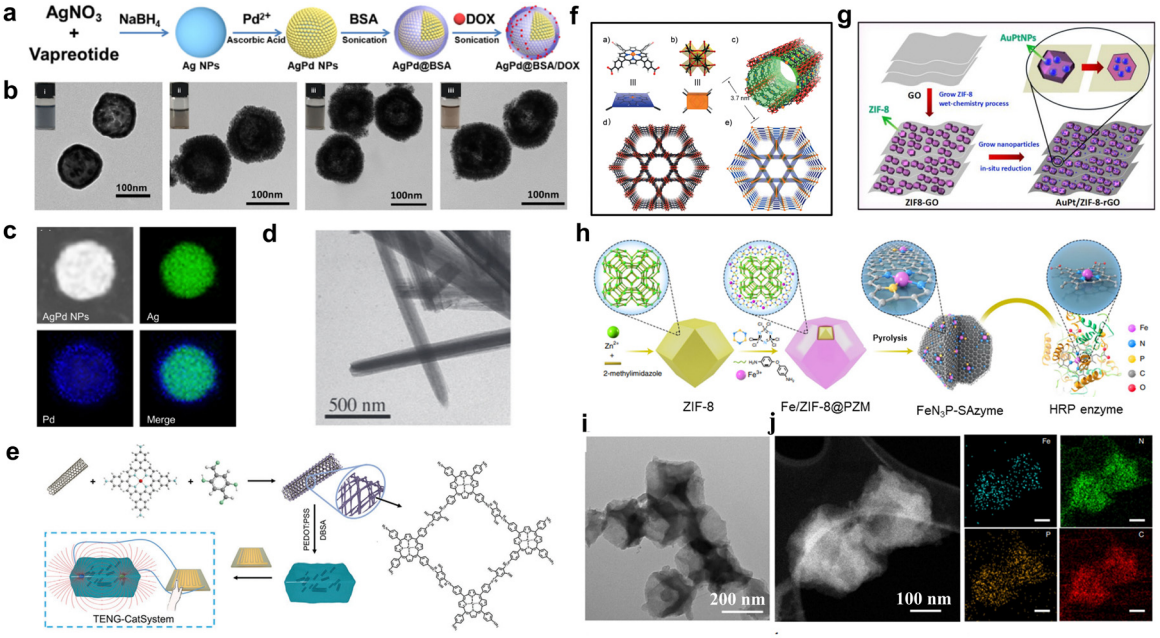

Fig. 2 (a) Schematic of the synthesis of AgPd@BSA/DOX. (b) TEM images during the synthesis process: (i) Ag NPs, (ii) AgPd NPs, (iii) AgPd@BSA, and (iv) AgPd@BSA/DOX. (c) SEM image and elemental mapping images of AgPd NPs. Adapted with permission.[30] Copyright 2020, Elsevier. (d) TEM images of V_2O_5 nanowires. Adapted with permission.[33] Copyright 2010, Wiley. (e) Schematic of the preparation of COF-CNT. Adapted with permission.[34] Copyright 2021, Wiley. (f) PCN-222(Fe) structure with POD-like activity. Adapted with permission.[35] Copyright 2012, Wiley. (g) Schematic of the synthesis process of AuPt/ZIF-8-rGO. Adapted with permission.[36] Copyright 2019, the American Chemical Society. (h) Illustration of the preparation process of FeN_3P-SAzyme. (i) TEM image of HAADF-STEM. (j) Corresponding EDS mapping images of FeN_3P-SAzyme. Adapted with permission.[37] Copyright 2021, Nature Portfolio.

activity, Li *et al.* reported a bimetallic $CuCo_2S_4$ nanozyme that show significant POD-like activity under neutral conditions, and its catalytic activity is much higher than that of single-metal CuS and CoS nanoparticles.[41]

2.3. Carbon-based nanozymes

Carbon-based nanomaterials including carbon nanodots, graphenes, diamonds, carbon nanotubes, fullerenes, and graphene quantum dots have also been found to have enzyme-like activities. The different hybridization states of carbon atoms (sp, sp^2 and sp^3) lead to great differences in the structure and physicochemical properties of carbon materials. As a non-metallic nanozyme, carbon-based nanozymes have a wide range of applications in the field of enzyme-like catalysis due to their high stability and low cost.[42,43]

The POD-like activity of graphenes was first reported by Qu *et al.* in 2010 and used for the detection of glucose.[44] In the enzyme-like catalytic process of graphenes and graphene derivatives, oxygen-containing functional groups such as –OH, –COOH, and epoxides, rich in surface or edge sites, play a very important role in catalytic activity. In 2010, Song *et al.* reported that single-walled carbon nanotubes have potential peroxidase activity to catalyze the oxidation of 3,3′,5,5′-tetramethylbenzidine (TMB) in the presence of H_2O_2, enabling detection of DNA up to 1 nM.[45] Since carbon materials such as carbon quantum dots and carbon nanotubes also have similar oxygen-containing functional groups, this conclusion also applies to the catalytic process of these materials. Similar to graphenes, carbon nanotubes are mainly used to mimic peroxidase during catalysis (Fig. 2e). In the study of amorphous carbon mimetic enzymes, the activity of amorphous carbon nanozymes can be regulated by adjusting the amount and type of heteroatoms incorporated.[46,47] One of the most common methods is N-doping. For example, Fan and his team created a nanozyme with multiple enzymatic activities using N-doped porous carbon spheres. The introduction of N renders this nanozyme POD-like activity, which allows it to regulate the intracellular levels of reactive oxygen species (ROS).[48]

2.4. Metal–organic framework nanozymes

MOFs are a class of porous coordination polymers formed by the coordination of inorganic metal centers and organic ligands. MOFs have the characteristics of unique chemical composition, orderly porous structure, large specific surface area and adjustable structure. MOFs are highly diverse due to the variety of metal nodes and organic ligands they can contain. As a result, they have been applied in various fields including chemical catalysis, gas separation, and drug delivery. In the area of enzyme-like catalysis, MOFs can exhibit different catalytic activities and types of catalysis by carefully selecting the metal centers and organic ligands used in their construction.[49,50] In 2012, Feng *et al.* first reported the POD-like activity of the zirconium-based porphyrin MOFs (PCN-222), the MOF with different open metal sites and a super-large one-dimensional pore structure formed by the coordination of Zr6 clusters with porphyrins, and they introduced different metal sites (Fe, Co, Mn, Ni, Cu, and Zn) into the metal porphyrin ligands and explored their catalytic activity. PCN-222(Fe) was found to exhibit the highest POD-like activity in the solution system, enabling biomimetic oxidation of a range of substrates

(Fig. 2f). Zhang *et al.* prepared ZIF-8-graphene oxide (ZIF-8-GO) by a wet chemical method, further introduced $AuCl_4^-$ and $PtCl_4^{2-}$, and obtained ZIF-8-rGO with AuPt nanoparticles by a reduction method, which showed enhanced peroxidase activity for the detection of H_2O_2 in human serum samples with ideal performance (Fig. 2g). Compared to metal-based, metal oxide/sulfide-based, and carbon-based nanozymes, MOF-based nanozymes offer unique advantages in mimicking the types of natural enzyme activities. This is due to their adjustable metal nodes and ligands, which allow them to exhibit a wider range of catalytic activities beyond just oxidoreductase activities. This characteristic is of great significance for expanding the potential applications of nanozymes.[51] The materials based on MOFs are becoming a powerful tool in the detection of common biomolecules. For example, Lu *et al.* developed a simple yet effective biosensor based on ZIF-67 loaded with bi-enzymes of glucose and hexokinase (HEX) for effective detection of ATP.[52] It paved the path for real-time monitoring of ATP released by cells, which will aid in understanding tumor cell glycolysis and immune responses. Zhao *et al.* synthesized CuO/C at different temperatures using metal–organic frameworks as sacrificial templates to achieve the detection of glucose in serum/saliva samples.[53] These make MOF materials attract widespread attention in the biomedical field.

2.5. Single-atom nanozymes

Single-atomic nanozymes (SAzymes) refer to a new type of catalyst that anchors isolated metal atoms with catalytic activity to solid supports. SAzymes have uniformly dispersed catalytically active sites, which provide a good opportunity to reveal the structure–activity relationship of catalytically active sites and precisely control the geometric and electronic properties of catalytically active sites. It has the advantages of maximizing the utilization efficiency of metal atoms, high catalytic activity and high stability. Most of the SAzymes developed at this stage use carbon-based materials as carriers to anchor metal atoms through nitrogen to form M–N–C SAzymes.[54] M–N–C SAzymes have an active site of $M–N_x$, which is very similar to that of native metalloproteinases, and many researchers have focused on the development of various types of M–N–C-type SAzymes for biomimetic enzyme catalysis.[55,56] This class of SAzymes with a definite active structure of $M–N_x$ has inherent advantages in elucidating the catalytic mechanism of nanozymes, overcoming the shortcomings of traditional nanozymes prepared based on trial-and-error strategies.[57]

By adjusting the types of metal atoms and coordination atoms, the geometric structure and electronic structure of the active sites of SAzymes can also be optimized, so as to achieve controllable regulation of the catalytic activity of enzymes. It has attracted increasingly more attention from researchers. Wang *et al.* used ZIF-8 as a precursor and introduced a molybdenum metal (Mo) source component into ZIF-8 through an *in situ* assembly strategy, and Mo-doped ZIF-8 calcined at different temperatures to obtain single-atom Mo nanozymes with different coordination numbers ($Mo_{SA}–N_x–C$, x = 2, 3, or 4). The comparison of enzyme kinetics showed that $Mo_{SA}–N_3–C$ exhibited the highest POD-like activity.[58] To further optimize the coordination environment of metal sites, Ji *et al.* also used ZIF-8-derived carbon carriers to design Fe SAzymes with a $Fe–N_3P_1$ site, which exhibited catalytic activity and enzyme kinetics comparable to that of natural peroxidase (Fig. 2h–j).

3. Strategies for regulating the activity of POD-like nanozymes

3.1. Composition

The composition control of nanozymes opens up the possibility of tuning their catalytic activity. The methods to modulate the activity of POD-like nanozymes by changing the composition can be broadly classified into two categories: (1) coating or growing materials with high POD-like activity on less active surfaces, and (2) doping another element into the lattice of the nanomaterial to form a solid solution. Some noble metal nanoparticles (*e.g.*, iridium, ruthenium, and platinum) have been shown to have excellent POD-like activity.[59] By coating or growing highly active noble metal nanoparticles on less active materials, not only their POD-like activity can be enhanced, but also the atomic utilization efficiency of noble metals can be improved. For example, Xia *et al.* obtained Pa–Ir core–shell cubes by depositing a layer of Ir atoms on the outer layer of Pa nanocubes. The POD-like activity of Pa–Ir nanocubes was enhanced by 20-fold and 400-fold compared to that of Pa cubes and HRP, respectively (Fig. 3a and b). In addition, noble metal nanoparticles have been used to modulate the POD-like activity of carbon-based or metal oxide-based nanomaterials, which not only enhances the POD-like activity of less active carbon or metal oxide-based nanomaterials, but also improves the catalytic cycling stability of metal nanoparticles.[60] In addition, a large number of studies have demonstrated synergistic effects between different components in composite nanomaterials. For example, Pt/cubic cerium oxide was prepared by *in situ* deposition of Pt nanoparticles on the surface of cubic cerium oxide, and the composite Pt/cubic cerium oxide exhibited a higher catalytic activity than a mixture of Pt and CeO_2 of the same mass, thanks to the metal-carrier interactions between the Pt particles and cerium oxide.[61]

Doping of other elements into the lattice of nanomaterials is another effective method to enhance the POD-like activity[65,66] and the enhanced POD-like activity is attributed to the alteration of the electronic structure of the original material by the doped elements. Hu *et al.* doped heteroatomic nitrogen into reduced graphene oxide (rGO) and mesoporous carbon, and the POD-like activity was increased by more than 100 and 60 times, respectively (Fig. 3c and d). In order to further improve the POD-like activity of carbon nanomaterials, researchers have successfully synthesized sulfur/nitrogen co-doped or nitrogen/boron co-doped carbon nanomaterials, which have a stronger POD-like activity than that of nitrogen doping alone.[67] In addition to carbon materials, the POD-like activity of metal oxides can be enhanced by elemental doping. For example, transition metals were doped into the lattice of cerium oxide (CeO_2) nanoparticles to form $M_xCe_{1-x}O_{2-\delta}$ solid solutions

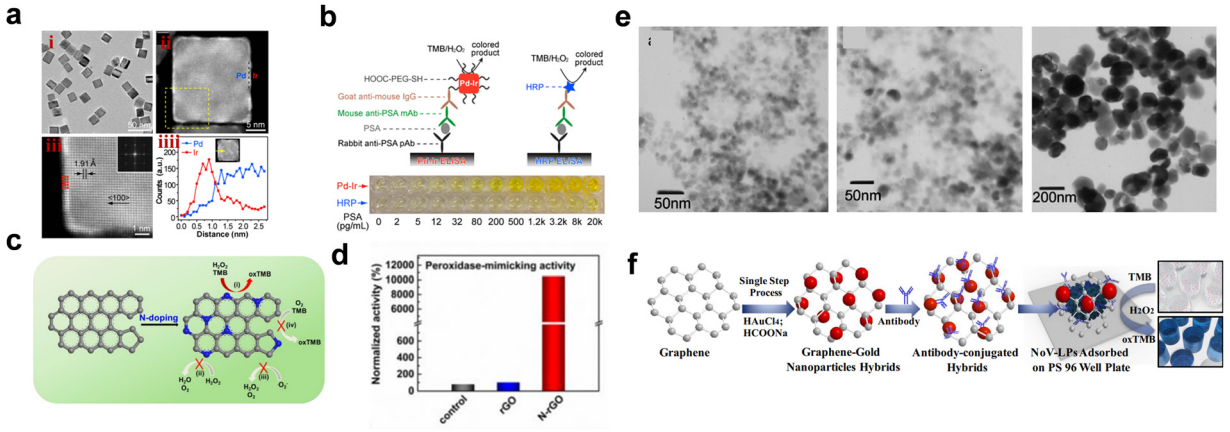

Fig. 3 (a) Structural and compositional analyses of the Pd–Ir core–shell cubes. (i) TEM image of the sample. (ii) and (iii) HAADF-STEM image of an individual particle. (iv) Line-scan EDX spectra of elemental Pd and Ir. (b) Detection of PSA with Pd–Ir cube-based ELISA and conventional HRP-based ELISA. Adapted with permission.[62] Copyright 2015, the American Chemical Society. (c) Schematic of the POD-like activity of N-rGO. (d) Normalized peroxidase-mimicking activities of rGO and N-rGO-5. Adapted with permission.[46] Copyright 2018, the American Chemical Society. (e) TEM images of Fe_3O_4 NPs with different average diameters. Adapted with permission.[63] Copyright 2018, Elsevier. (f) Schematic of the one-step preparation of Grp-Au NP hybrids using Graphene flakes, HCOONa and $HAuCl_4$. Adapted with permission.[64] Copyright 2017, Elsevier.

(M stands for transition metal elements). In these CeO_2-based doped materials, the Mn-doped cerium solid solution exhibits significantly enhanced POD-like activity.[68]

3.2. Size

Generally speaking, size has an important effect on the properties of different nanomaterials. In most cases, nanozymes with smaller particle sizes show more activity in catalytic reactions due to their larger specific surface area. Therefore, the POD-like activity of nanomaterials is closely related to their size.[69] Many studies have shown that the smaller the size, the higher the POD-like activity of the material. Gao *et al.* demonstrated that the catalytic activity of Fe_3O_4 nanoparticles is size-dependent, and the corresponding POD activity of Fe_3O_4 nanoparticles decreases as the size of Fe_3O_4 nanoparticles (30, 150, and 300 nm) increases. Smaller Fe_3O_4 nanoparticles have higher catalytic activity due to their larger specific surface area, which, in turn, allows them to expose more catalytically active sites. Peng *et al.* prepared Fe_3O_4 nanoparticles of three sizes (11, 20 and 150 nm) and similarly found that the POD-like activity of Fe_3O_4 decreases with the increase in its size (Fig. 3e).[63] Ahmed *et al.* obtained Au nanoparticles with particle sizes of 10, 80, 200 and 500 nm by *in situ* reduction on the surface of graphenes as a substrate, and it was also found that the smaller the size of Au nanoparticles, the higher the POD-like activity (Fig. 3f).[64]

Therefore, the size can change the specific surface area as well as other surface properties of nanomaterials, which, in turn, affects the POD-like activity.[70] The phenomenon has been similarly found in some noble metal nanozymes. For example, compared to Pt nanozymes synthesized from guanine-rich oligonucleotides (1.8 nm in size), Pt nanozymes synthesized from cytosine-rich oligonucleotides (2.9 nm in size) showed better POD-like activity. This study showed that more metal Pt^0 was present on the surface of 2.9 nm Pt nanozymes, resulting in high POD-like activity, whereas more Pt^{2+} was present on the surface of the 1.8 nm Pt nanozymes.

3.3. Crystal surfaces

In terms of regulating the catalytic activity of enzymes, controlling the exposure of the crystal plane of materials is also a very effective means. Generally speaking, adjusting the morphology of materials is a common strategy in the process of crystal plane manipulation, and different morphologies often expose different crystal planes. These crystals with different atomic arrangements and unsaturated coordination sites exhibit different adsorption energy, reaction energy and activation energy barriers to the same substrate, and have different catalytic activities. Since nanomaterials with different morphologies have different crystal planes, the POD-like activity of nanozymes can be adjusted by regulating the morphology. Liu *et al.*[71] obtained three types of Fe_3O_4 nanocrystals with different morphologies (clustered spheres, octahedra and triangles) by a hydrothermal method, respectively. This study showed that the clustered spheres with the exposed {311} facets exhibited the highest POD-like activity, the triangular nanocrystals with the {200} facets exhibited relatively weak POD-like activity, and the octahedral Fe_3O_4 with the {111} facets had the lowest catalytic activity. Many studies have shown that metal nanoparticles with these facets are usually more reactive than those with low-index facets due to the abundance of ligand-unsaturated atomic steps and frameworks, *etc.*, on the high-index facets[72] Wu *et al.* prepared Pd–Pt core–frame nanodendrites by growing dense arrays of Pt branches on a Pd core by wet etching (Fig. 4a). In order to further improve the catalytic activity, the less active Pd nanocore structures therein were selectively etched away to form Pt frame structures capable of exposing more active sites and high index facets (*i.e.*, {110} and {311} facets). In addition, density functional theory calculations confirmed the different POD-like activities of the materials with different crystallographic facets. Li *et al.* investigated the effect of different crystal facets on the POD-like activity of Au nanocrystals by density-functional theory calculations and found that Au nanozymes with the {111}, {110} and {211} facets followed the same catalytic mechanism and had

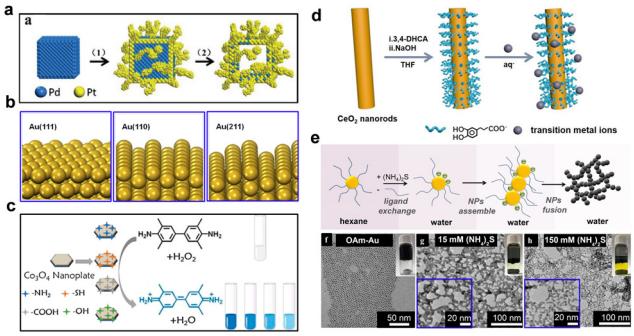

Fig. 4 (a) Construction of Pt hollow nanodendrites from Pd nano-cubes. Adapted with permission.[73] Copyright 2018, Wiley. (b) Structures of Au(111), Au(110), and Au(211) surfaces. Adapted with permission.[74] Copyright 2015, Elsevier. (c) Co_3O_4 nanozymes modified with different functional groups. Adapted with permission.[75] Copyright 2021, the American Chemical Society. (d) Schematic of engineering nanoceria by transition metal ion chelation for enhanced peroxidase mimics. Adapted with permission.[28] Copyright 2021, Elsevier. (e) Schematic of the proposed mechanism for Au gel preparation. (f) TEM images of as-prepared OAm-Au. TEM images of aerogels produced in (g) 15 mM and (h) 150 mM $(NH_4)_2S$. Adapted with permission.[76] Copyright 2019, the American Chemical Society.

the same rate-determining step. Based on the activation energy barrier of the rate-determining step, the {111} facet with the highest energy barrier had the lowest catalytic activity, while the Au nanozymes with the {211} facet had the highest catalytic activity (Fig. 4b).

3.4. Surface modification

Since the reaction between nanozymes and substrates generally occurs on the surface of the material, properties such as surface charge, exposure of active sites, and substrate binding ability can be modulated by modifying the surface of the material.[75] The diverse modifications encompass a broad spectrum, including group modification, ionic modification, and polymer modification, among others. Each of these strategies offers unique advantages in tailoring the properties and functionalities of the material. Through surface modification, nanozymes can be endowed with new types of catalytic activities, improved enzyme-like catalytic specificity, or inhibition of a particular catalytic reaction activity. Therefore, surface modification is a highly flexible and controllable strategy to tune the activity of nanozymes. Liu *et al.* reported that the catalytic efficiency of DNA-encapsulated iron oxide nanoparticles as peroxidase mimics was approximately 10-fold higher than that of bare NPs.[77] The DNA membrane layer not only enhances the binding ability to the TMB amino group *via* hydrogen bonding but also provides a π–π stacking interaction between nucleobases and the TMB benzene ring, which effectively strengthens the affinity of the Fe_3O_4 NPs toward TMB. Huo *et al.* modified Co_3O_4 nanoplates with amino (NH_2–Co_3O_4), carboxyl (COOH–Co_3O_4), hydroxyl (OH–Co_3O_4), and sulfhydryl (SH–Co_3O_4) groups, respectively, and systematically investigated their catalytic activities (Fig. 4c). Except for the hydroxyl group, all functional groups showed positive enhancement of POD-like activity, with NH_2–Co_3O_4 nanoplates showing the greatest enhancement of POD-like activity. According to Huo *et al.*, the effect of functional groups on the electron transfer capacity of nanozymes is crucial for modulating their catalytic performance. Yue *et al.* prepared functionalized ceria nanorod catalysts M/CeO_2 ($M = Fe^{3+}$, Co^{2+}, Mn^{2+}, Ni^{2+}, Cu^{2+}, and Zn^{2+}) by chelating ceria nanorods on CeO_2 surfaces with metal ions.[28] All of these metal-chelated nanoceramics exhibited enhanced POD-like properties, with Mn(II)/CeO_2 displaying the optimal catalytic performance (Fig. 4d).

3.5. Surface valence state

The valence of elements on the surface of nanozymes is closely related to the catalytic activity of the enzyme, and the valence of different elements leads to changes in catalytic activity and catalytic type. For instance, Fan *et al.* achieved the first surface valence control of Au-based nanozymes (Fig. 4e–h). In their system, the catalytic efficiency of substrate oxidation (TMB and H_2O_2) decreased as the proportion of Au(I) complexes in the Au aerogel decreased.[76] By tuning the copper state from Cu^0 to Cu^{2+}, Xi *et al.* found that the POD-like activity of copper/carbon nanozymes was closely related to the Cu state.[69] Wang *et al.* reported that the POD mimetic activity of Ni-based nanozymes was related to the oxidation state of Ni.[78] In their study, the catalytic performance of porous $LaNiO_3$ chalcogenides was 58-fold higher than that of NiO and 22-fold higher than that of Ni NPs, suggesting that Ni-based nanomaterials exhibit POD-like properties that depend on the Ni oxidation state. Furthermore, they demonstrated the modulation of catalytic activity by varying the proportion of Ni^{3+} through the comparison of $LaNiO_3$–H_2 and $LaNiO_3$ nanocubes.

3.6. External factors

In addition to the aforementioned regulatory strategies, several external factors, including pH, temperature, biologically relevant molecules, salt ion concentration, and light/acoustic stimulation, can significantly influence the POD-like catalytic activity. For instance, the incorporation of ATP resulted in significant enhancement in the POD-like activity of Au NPs.[79,80] In addition, the POD-like activity exhibited pH dependence. Based on this, Sanjay Singh group reported that nanoparticles showed POD-like activity at acidic pH, and the POD-like activity disappeared under neutral conditions. Loading them in pH-responsive microcapsules becomes a vital strategy to avoid exposure to the acidic environment of stomach.[81] Under acidic conditions, certain oxides such as Fe_3O_4 exhibit properties reminiscent of POD-like activity. Conversely, under neutral and alkaline conditions, the activities of catalase and superoxide dismutase predominate. The introduction of external light can manipulate the nanozymatic reaction temperature towards the optimal range *via* the photothermal effect of the material, thereby accelerating the catalytic reaction rate. Alternatively, it can directly modulate the electron population and transfer rate on the surface of materials, such as through localized plasmonic resonance to stimulate hot electron generation or light-induced electron–hole separation to enhance carrier concentration. These strategies, which leverage

external factors to optimize the catalytic performance of nanozymes, represent highly efficacious regulatory approaches.

4. Biomedical applications

4.1. Biosensing

POD-like nanozymes play an important role in signal generation and amplification of biosensors. Thus far, various types of biosensing technologies including colorimetry, fluorescence, chemiluminescence, electrochemistry, and surface-enhanced Raman technology have been successfully constructed based on different signal modes catalyzed by nanozymes. The sensing strategies of these sensors can be broadly classified into two categories: the first utilizes nanozymes as signaling units to catalyze the reaction between various chromogenic substrates and targets or their oxidation products, with the color intensity of the chromogenic substrates being proportional to the concentration of the target. The second category involves inhibiting or enhancing the catalytic efficiency of nanozymes through the presence of the target, allowing the analyte content to be indirectly reflected by either the initial color change of the chromogenic substrate or the reaction residue. We summarize the applications of POD-like nanozymes in biosensing in Table 2.

4.1.1. Colorimetric biosensing. Colorimetric biosensing is a method of detecting biomolecules using the color changes produced by chemical reactions. Its principle is based on the color change produced after biological molecules react with specific reagents. Among the various sensing methods for

Table 2 POD-like nanozymes for biosensing applications

Materials	Sensing method	Sensing object	Linear range	Limit of detection	Ref.
MOFs-MIPs	Surface-enhanced Raman scattering	Trace diazinon	10 nmol L^{-1}–1.0 mmol L^{-1}	3.6 nmol L^{-1}	34
Ag NPs@CS-Hemin/rGO	Electrochemistry	CEA	20 fg mL^{-1}–200 ng mL^{-1}	6.7 fg mL^{-1}	36
Co-MOFs	Electrochemistry	miRNA	1.0×10^{-12}–1.0×10^{-6} mol L^{-1}	1.2×10^{-13} mol L^{-1}	49
Ir(III)/GO	Colorimetry	PIB	1.0×10^{-8}–3.0×10^{-7} mol L^{-1}	2.81×10^{-9} mol L^{-1}	55
MIL-3DG-75	Fluorescence	Xanthine	0–2.0×10^{-4} mol L^{-1}	1.4×10^{-9} mol L^{-1}	56
PdNPs@Fe-MOFs	Electrochemistry	miR-122	1.0×10^{-17}–1.0×10^{-14} mol L^{-1}	3.0×10^{-18} mol L^{-1}	61
Au NCs	Colorimetry	GSH	2.0×10^{-6}–2.5×10^{-5} mol L^{-1}	4.2×10^{-7} mol L^{-1}	81
GK-Pd NPs	Colorimetry	Glucose	1.0×10^{-5}–1.0×10^{-3} mol L^{-1}	6.0×10^{-6} mol L^{-1}	82
MoS_2NRs-Au NPs	Colorimetry	Cholesterol	4.0×10^{-4}–1.0×10^{-3} mol L^{-1}	1.5×10^{-5} mol L^{-1}	83
Fe-g-C_3N_4	Colorimetry	Glucose	5.0×10^{-7}–1.0×10^{-5} mol L^{-1}	5.0×10^{-7} mol L^{-1}	84
CS-$MoSe_2$ NS	Colorimetry	Hg^{2+}	0.025–2.5 μmol L^{-1}	0.0035 μmol L^{-1}	85
MOF-808	Colorimetry	AA	5.0×10^{-5}–1.03×10^{-3} mol L^{-1}	1.5×10^{-5} mol L^{-1}	86
MIL-53 (Fe) MOF	Colorimetry	Glucose	2.5×10^{-7}–2.0×10^{-5} mol L^{-1}	2.5×10^{-7} mol L^{-1}	87
GO@Au@MnO_2	Surface-enhanced Raman scattering	Glucose	1–10 μmol L^{-1}	0.114 μmol L^{-1}	88
Au@AuAg NPs	Fluorescence	H_2O_2	1.0×10^{-6}–4.0×10^{-4} mol L^{-1}	8.65×10^{-7} mol L^{-1}	89
Cu_2O@$Fe(OH)_3$	Fluorescence	Ochratoxin A	1 ng L^{-1}–10 μg L^{-1}	0.56 ng L^{-1}	90
V_2O_5	Fluorescence	AA	0.01–2.5 μmol L^{-1}	3 nmol L^{-1}	91
N-CDs-MnO_2	Fluorescence	Acid phosphatase	5–40 U L^{-1}	0.1 U L^{-1}	92
Borophene QDs	Fluorescence	Oxytetracycline	0–1.0×10^{-4} mol L^{-1}	1.14×10^{-6} mol L^{-1}	93
hemin@CD	Fluorescence	H_2O_2	1.7×10^{-7}–3.33×10^{-4} mol L^{-1}	1.5×10^{-7} mol L^{-1}	94
N, Fe-CDs	Fluorescence	UA	8.0×10^{-7}–1.33×10^{-4} mol L^{-1}	4.9×10^{-7} mol L^{-1}	95
Cu-MOF	Fluorescence	Glucose	1.0×10^{-5} – 1.0×10^{-4} mol L^{-1}	4.1×10^{-7} mol L^{-1}	96
Cu–N/C	Fluorescence	AA	1.0×10^{-5}–1.3×10^{-4} mol L^{-1}	7.0×10^{-7} mol L^{-1}	97
BSA@AuNCs	Chemiluminescence	GSH	50.0–5000.0 nmol L^{-1}	5.2 nmol L^{-1}	98
Pt/Ag	Chemiluminescence	Glucose	1–500 μmol L^{-1}	0.35 μmol L^{-1}	99
Au NPs	Chemiluminescence	AFP	5–70 ng mL^{-1}	2.5 ng mL^{-1}	100
$Co(OH)_2$	Chemiluminescence	Enrofloxacin	0.0001–1000 ng mL^{-1}	0.041 pg mL^{-1}	101
$CoMoO_4$	Chemiluminescence	Dopamine	10–500 nmol L^{-1}	1.98 nmol L^{-1}	102
Fe_3O_4M NPs	Chemiluminescence	CA125	0–10 μmU mL^{-1}	8.0 μU mL^{-1}	103
HRP-CdTe	Chemiluminescence	Triphosadenine	50–231 μmol L^{-1}	185 nmol L^{-1}	104
Ni/Co-MOF	Chemiluminescence	Florfenicol	0.0001–1000 ng mL^{-1}	0.033 pg mL^{-1}	105
Cu-TCPP(Co) MOF	Chemiluminescence	Thrombin	8.93×10^{-13}–5.9×10^{-10} mol L^{-1}	2.18×10^{-13} mol L^{-1}	106
Co SAzyme	Chemiluminescence	5-Fluorouracil	0.001–1000 ng mL^{-1}	0.29 pg mL^{-1}	107
Co SADCs	Chemiluminescence	Carbendazim	1.0 pg mL^{-1}–25 ng mL^{-1}	0.33 pg mL^{-1}	108
Pt/PdCu	Electrochemistry	SCCA	0.0001–1 ng mL^{-1}, 1–30 ng mL^{-1}	25 fg mL^{-1}	109
Ni–Co–P NSs	Electrochemistry	DA	0.3–50 μmol L^{-1}	0.016 μmol L^{-1}	110
NiCo-P@NiCo-LDH	Electrochemistry	Isoprenaline	0.5–2110 μmol L^{-1}	0.17 μmol L^{-1}	111
MoS_2/Au	Electrochemistry	Tau protein	0.1 pg mL^{-1}–100 ng mL^{-1}	33.4 fg mL^{-1}	112
Fe_3O_4@SiO_2	Electrochemistry	CEA	0.001–80 ng mL^{-1}	0.0002 ng mL^{-1}	113
Au–Fe_3O_4	Electrochemistry	α-Fetoprotein	0.01–40 ng mL^{-1}	2.3 pg mL^{-1}	114
MWCNT-PDDA-AuPd	Electrochemistry	Bisphenol A	0.18–18 μmol L^{-1}	60 nmol L^{-1}	115
AuNFs/Fe_3O_4@ZIF-8-MoS_2	Electrochemistry	H_2O_2	5.0×10^{-6}–1.2×10^{-1} mol L^{-1}	0.9×10^{-6} mol L^{-1}	116
Fe_3C@C/Fe–N–C	Electrochemistry	H_2O_2	1.0×10^{-6}–6.0×10^{-3} mol L^{-1}	2.6×10^{-7} mol L^{-1}	117
Co-AcNC-3	Electrochemistry	Catechol	4.0–300.0 μmol L^{-1}	0.072 μmol L^{-1}	118
Au@Pt NPs	Surface-enhanced Raman scattering	Dichlorvos	20–2000 μg L^{-1}	20 μg L^{-1}	119
Cu_2O@Au	Surface-enhanced Raman scattering	Aflatoxin B1	0.001–100 ng mL^{-1}	0.7 pg mL^{-1}	120
SiO_2@Au@Ag	Surface-enhanced Raman scattering	α-Fetoprotein	0.2–22 ng mL^{-1}	0.1 ng mL^{-1}	121
GO	Surface-enhanced Raman scattering	PSA	0.5–500 pg mL^{-1}	0.23 pg mL^{-1}	122

nanozymes, colorimetric assays are the most prevalent, and these assays leverage the ability of nanozymes to catalyze the chemical reactions involving chromogenic substrates such as TMB and ABTS, leading to a visible color change that serves as an output signal. These signals can be qualitatively assessed through visual inspection or quantitatively measured using equipment like UV spectrophotometers or microplate readers. Recently, with the ascendancy of point-of-care detection technologies, the outputs of such sensors have been integrated with more affordable portable devices, such as smartphones.

Colorimetric sensors based on POD-like activity represent the most widely reported category. For instance, Zheng *et al.* successfully synthesized a novel and stable MOF (MOF-808) that exhibits remarkable POD-mimicking catalytic activity under alkaline, neutral, and acidic conditions.[86] This material effectively catalyzes the oxidation of TMB in the presence of H_2O_2, generating distinct color changes. Building upon the excellent catalytic performance of the MOF-808 nanozyme, a novel, simple, and sensitive colorimetric biosensor was successfully developed. Moreover, Huang *et al.* prepared chitosan-functionalized molybdenum selenide nanosheets and employed them as recognition elements. Intriguingly, Hg^{2+} ions can activate the nanozyme activity of these nanosheets, thereby facilitating the oxidation of TMB and yielding a colorimetric response. This breakthrough enabled the establishment of a colorimetric biosensor for the detection of Hg^{2+} (Fig. 5a). Additionally, Zhang *et al.* utilized synthetic Fe_3O_4 nanoparticle clusters (Fe_3O_4 NPC) as nanozymes to amplify colorimetric signals.[123] By incorporating aptamers and the glycopeptide antibiotic vancomycin (Van), they developed a colorimetric biosensor capable of recognizing *Listeria monocytogenes* (*L. monocytogenes*), a Gram-positive bacterium (Fig. 5b). Furthermore, Xia *et al.* devised a Ni–Pt nanozyme that boosts the catalytic activity 10 000 times higher than that of natural peroxidase.[124] When applied to the enzyme-linked immunosorbent assay (ELISA) for the carcinoembryonic antigen, this nanozyme achieved an ultrasensitive detection limit of 1.1 pg mL^{-1}, which is hundreds of times lower than the limit achieved by traditional ELISA immunoassays relying on natural enzymes (376 pg mL^{-1}). This demonstrates that enhancing the catalytic activity of nanozymes is pivotal in improving the detection sensitivity (Fig. 5c).

4.1.2. Fluorescence biosensing. Fluorescence biosensing is a sensing technology that uses the properties of fluorescent substances to detect specific biomolecules. When a fluorescent substance binds to a target biomolecule, its fluorescence properties (such as fluorescence intensity, emission wavelength, or fluorescence lifetime) change. By detecting these changes, the high-sensitivity detection of target biomolecules can be achieved.

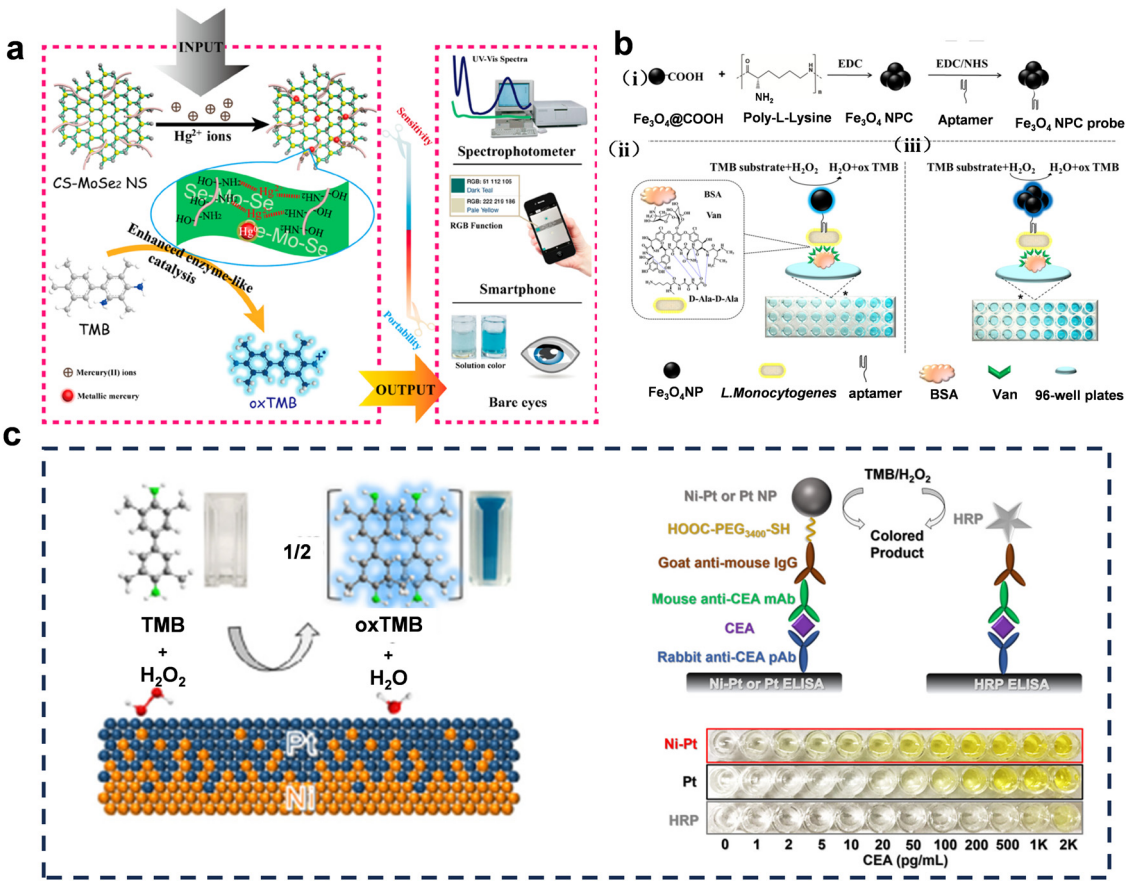

Fig. 5 (a) Illustration of the CS-$MoSe_2$ NS-based versatile colorimetric detection of mercury ions. Adapted with permission.[85] Copyright 2019, the American Chemical Society. (b) (i) Schematic of the preparation of Fe_3O_4 NPC. (ii) Principle of the Fe_3O_4 NP-based biosensor and (iii) Fe_3O_4 NPC-catalyzed signal amplification biosensor. Adapted with permission.[123] Copyright 2016, Elsevier. (c) High-performance Ni–Pt nanozyme applied in the detection of carcinoembryonic antigen by ELISA. Adapted with permission.[124] Copyright 2021, the American Chemical Society.

It is primarily based on target analyte-mediated fluorescence enhancement ("on") or fluorescence quenching ("off"). In recent years, nanozyme-based fluorescent biosensors have also gained extensive research interest due to their excellent performance in fluorescence signal generation and amplification. They have been widely used in many fields.[125] For example, Lin *et al.* synthesized a MIL-53(Fe) nanozyme with POD-like catalytic activity (Fig. 6a). Under the catalysis of H_2O_2 by the MIL-53(Fe) nanozyme, a fluorescent product was generated and the fluorescence intensity of the sensing system is related to the concentration of H_2O_2. Furthermore, a simple, stable, cost-effective and sensitive method for the detection of glucose in normal and diabetic human serum samples is constructed by using the label-free MIL-53(Fe) nanozyme and glucose oxidase for the construction of an enzyme cascade reaction. Fu *et al.* constructed a ratiometric fluorescence sensing platform based on POD-like nanozymes for the detection of glucose (Fig. 6b).[106] First, glucose oxidase catalyzes glucose and provides H_2O_2 for subsequent reactions, followed by the conversion of the fluorescent substrate *o*-phenylenediamine (OPD) to the fluorescent species 2,3-diamino phenylhydrazine (DAP) catalyzed by peroxidase activity of copper-doped carbon-based nanozymes with maximum emission at 558 nm. Due to the presence of fluorescence internal filtration, DAP quenched the fluorescence of Mg/N-doped carbon quantum dots (Mg-N-CQDs) at 444 nm, and within a certain range, the proportional fluorescence signal I_{558}/I_{444} increased linearly with the glucose concentration, from which the concentration of glucose could be quantified. The method was validated in human serum samples with a detection limit of 1.56 μmol L^{-1}.

4.1.3. Chemiluminescence biosensing. Chemiluminescence sensing is a kind of sensing technology based on the light signal generated *via* chemical reactions. This luminescence phenomenon is usually caused by the energy released in a chemical reaction to stimulate electrons to jump to a higher energy level, and when these electrons fall back to a lower energy level, they release photons, resulting in a light signal. These light signals can be captured by sensors and converted into electrical signals for quantitative or qualitative analysis. Chemiluminescence biosensors have emerged as promising analytical tools due to their independence from excitation light sources and complex spectroscopic systems, making detection equipment relatively simple and cost-effective. The advent of nanozymes has sparked interest in advancing chemiluminescence sensors. Luminol, the prevalent chemiluminescent substrate, emits intense blue light upon oxidation, lasting for up to several minutes. Its oxidation necessitates the presence of H_2O_2, making it an ideal substrate for nanozymes with POD-like activity. For example, Au NPs, Ag NPs, and MIL-type MOFs, endowed with POD-like catalytic activity, have been harnessed as biomimetic components to catalyze the generation of fluorescent signals in the H_2O_2-luminol system, fostering the development of chemiluminescent biosensors.[128] Luo *et al.* developed a novel MOF-based solid catalyst, Hemin@HKUST-l, by encapsulating heme chloride (Hemin).[129]

This catalyst exhibits robust POD-like activity, efficiently catalyzing the production of fluorescence signals in the H_2O_2-luminol system, thereby enabling the creation of a chemiluminescent biosensor with high selectivity and sensitivity.[129] As shown in Fig. 6c, Yang *et al.* constructed an off-chemiluminescence

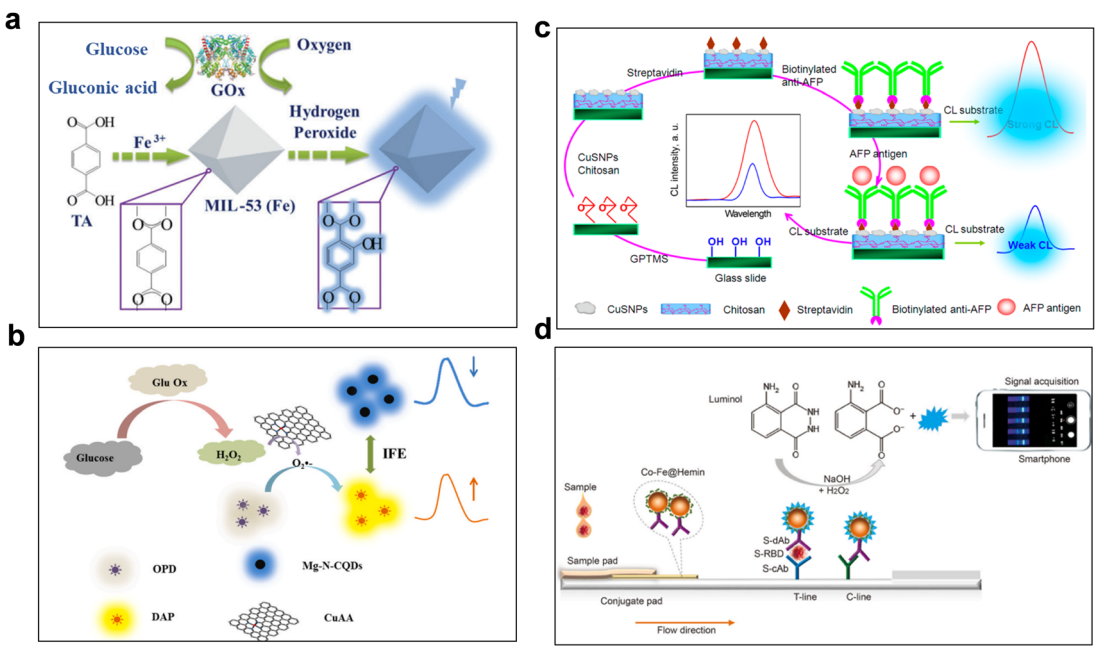

Fig. 6 (a) Principle of fluorescence detection of glucose based on the bifunctional MIL-53(Fe) nanozyme. Adapted with permission.[126] Copyright 2018, the Royal Society of Chemistry. (b) Illustration of the ratiometric fluorescence sensing platform for glucose. Adapted with permission.[127] Copyright 2022, the American Chemical Society. (c) Schematic exhibition of fabrication process of the immunosensor and label-free CL immunoassay protocol. Adapted with permission.[26] Copyright 2016, the American Chemical Society. (d) Schematic of the nanozyme chemiluminescence paper test for SARS-CoV2 S-RBD antigen. Adapted with permission.[14] Copyright 2021, Elsevier.

immunosensor for the detection of alpha-fetoprotein antigen. First, CuS nanoparticles were used as peroxidase mimics and carrier materials to be immobilized on glass slides by chitosan crosslinking. Subsequently, streptavidin was modified on the slides to capture biotinylated antibodies, resulting in an interface that exhibited good catalytic activity and triggered intense chemiluminescence in the H_2O_2-luminol system. Upon capturing the alpha-fetoprotein antigen as it flowed through the sensing interface, the formed antibody–antigen complex hindered the free diffusion of the chemiluminescent substrate to the signaling interface, leading to a decrease in chemiluminescence intensity with the increase in antigen concentration. Furthermore, in view of the rapid spread of epidemic virus globally, Yan *et al.* established a highly sensitive chemiluminescence rapid test strip platform using a Co–Fe@hemin peroxide nanozyme. This platform enables rapid and sensitive detection of SARS-CoV2 virus within 16 minutes, with a detection limit of 360 $TCID_{50}$ per mL, comparable to that of the ELISA method (Fig. 6d). This advancement is instrumental in early virus screening and epidemic prevention and control efforts.

4.1.4. Electrochemical biosensing. Electrochemical sensing is a detection technology based on electrochemical principles, which uses the electrical signals generated by substances during chemical reactions to detect and analyze target substances. As a subclass of chemical sensors, electrochemical biosensors include two components: target recognition unit and electrochemical signal transduction unit. Typically, in the presence of the analyte to be measured, the target recognition unit (*e.g.*, enzyme, antigen, *etc.*) first reacts with the analyte and subsequently transduces that recognition event into a detectable electrical signal. This electrical signal is typically positively or negatively correlated with the analyte concentration, allowing for qualitative or quantitative detection. Electrochemical biosensors have been widely used in pharmaceutical analysis, environmental monitoring, chemical analysis, bioanalysis, and clinical diagnosis due to their simple operation, low cost, good stability, and sensitive response. In order to further improve the analytical sensitivity of electrochemical biosensors, the modification of electrodes with more uniformly dispersed catalysts and electrocatalytic sites is a very effective strategy.[130] In recent years, various nanozymes (including Au NPs, Ag NPs, Pt NPs, Au@Pt NPs, AuPd@Au NPs, and Cu-MOF) have good enzyme-like catalytic activity, and have been widely used to catalyze electrochemical signal amplification and construct novel electrochemical biosensors. Based on nickel oxide nanoplate-modified screen-printed electrodes, Khairy *et al.* developed a new, simple and highly sensitive nanozyme electrochemical biosensor.

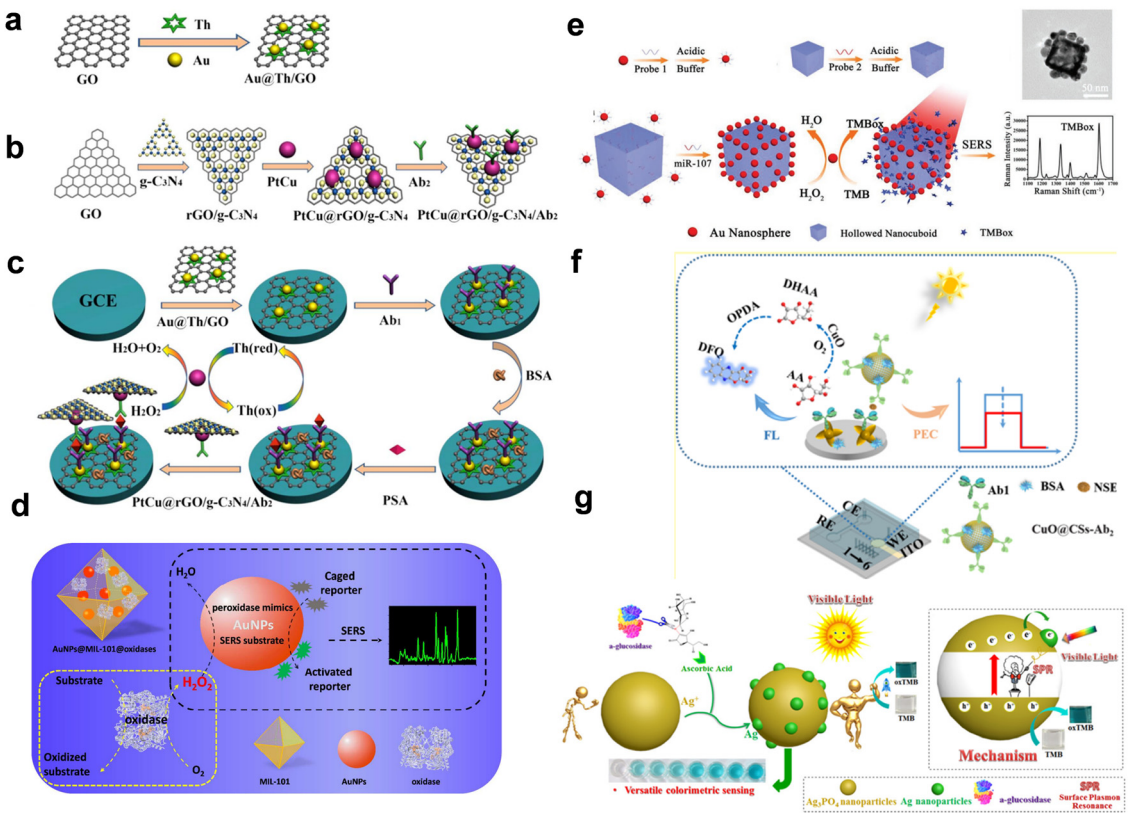

Fig. 7 (a) Schematic of the fabrication procedure of Au@Th/GO. (b) and (c) PtCu@rGO/g-C_3N_4/Ab_2 and the sandwich-type electrochemical immunosensor for PSA detection. Adapted with permission.[132] Copyright 2017, Elsevier. (d) Schematic of Au NPs@MIL-101@oxidases for efficient enzymatic cascade reactions. Adapted with permission.[133] Copyright 2017, the American Chemical Society. (e) Schematic of the triggered self-assembly of plasmonic nanostructures for miR-107 detection. Adapted with permission.[134] Copyright 2019, Wiley. (f) Copper oxide nanozymes as efficient multifunctional signal markers of photocurrent quenching of ZnO/Au/$AgSbS_2$ hybrid material. Adapted with permission.[135] Copyright 2022, the American Chemical Society. (g) Schematic of the colorimetric sensing strategy based Ag_3PO_4 nanozymes. Adapted with permission.[136] Copyright 2018, Elsevier.

This electrochemical biosensor has demonstrated good analytical performance (including good stability, high selectivity, and sensitivity) in the determination of OPs (p-thio) in vegetables, water, and human urine samples.[131] As shown in Fig. 7a–c, Feng *et al.* developed an ultra-sensitive sandwich electrochemical immunosensor for the quantitative detection of prostate-specific antigen (PSA) using PtCu@rGO/g-C_3N_4 nanozyme as a catalytic tag, with a detection limit of 16.6 fg mL^{-1}, demonstrating good stability and selectivity.[132]

4.1.5. Surface-enhanced Raman scattering biosensing. Surface-enhanced Raman scattering (SERS) biosensing is an advanced analytical method that combines surface-enhanced Raman scattering and biosensing techniques. When the molecules adsorb onto the surface of nanostructures of some specially prepared metals (such as Au, Ag, and Cu), the Raman scattering signal will be greatly enhanced, and this phenomenon is called SERS. Biosensing technology uses biomolecules (such as enzymes, antibodies, and nucleic acids) as recognition elements to detect and analyze target substances through their specific interactions with target molecules. Since Fleischmann *et al.* first found the abnormally enhanced Raman scattering of pyridine on a rough silver electrode, SERS technology has attracted a great deal of attention in biomedicine. SERS biosensors typically quantify targets by measuring changes in the Raman-labeled molecular signals. The analysis process involves target identification and capture, Raman nanoprobe labeling, and signal reading. In recent years, various SERS-based analytical platforms have been successfully established for the sensitive detection of various target molecules, using nanozymes to enhance SERS performance. For example, Jiang *et al.* developed a novel and efficient SERS substrate by modifying Ag NPs onto the surface of MIL-101(Fe) with POD-like activity using an *in situ* manufacturing strategy. The interaction between the MIL-101(Fe) nanozyme and high-density Ag NPs creates numerous Raman hotspots, resulting in high-performance SERS biosensors.[137] Hu *et al.* prepared Au NPs@MIL-101 nanozymes by growing Au NPs *in situ* within the thermostable and porous MIL-101 framework.[133] This nanozyme exhibits POD-like catalytic activity, enabling it to not only catalyze the oxidation of an inactive Raman reporter (recessive malachite green) into a SERS-active form (malachite green) in the presence of H_2O_2 but also serve as a robust SERS substrate for generating strong Raman signals. Leveraging its exceptional properties, the Au NPs@MIL-101 nanozyme was employed to construct SERS biosensors for monitoring glucose and lactate levels in living tissues (Fig. 7d). Furthermore, Trau *et al.* designed a nanozyme-based SERS sensing platform for detecting biomarker miRNAs. In the presence of the target miRNA, nucleic acid probe-labeled Au POD-like nanozymes are assembled onto a hollow nano-framework through base complementarity, forming plasmonic nanostructures.[134] The subsequent addition of TMB is catalyzed by the POD-like nanozymes, producing oxTMB as a Raman reporter. This strategy was validated in clinical urine samples, achieving a minimum detection limit of 0.7 fmol L^{-1} (Fig. 7e).

4.1.6. Other biosensing. In addition to the above-mentioned biosensors, other nanozyme-based biosensors such as photoelectrochemistry (PEC) and surface plasmon resonance (SPR) biosensors have been successfully developed. For example, Wu *et al.* developed a novel dual-mode microfluidic biosensing platform for the detection of ultrasensitive neuron-specific enolases using CuO nanozymes as PEC and fluorescence signal labels.[135] The PEC biosensors have a linear range of 0.0001–150 ng mL^{-1} and a limit of detection of 0.028 pg mL^{-1}, whereas the FL biosensors have a linear range of 0.001–150 ng mL^{-1} and a limit of detection of 0.25 pg mL^{-1} (Fig. 7f). In another study, Wu *et al.* reported an SPR biosensing strategy based on the precisely regulated Ag_3PO_4 nanozyme signal amplification of ascorbic acid (AA) for the screening of α-glucosidase inhibitors. This SPR biosensor provides ultra-sensitive colorimetric detection of α-glucosidase inhibitors with a detection limit of 10 nM and allows for visual detection of concentrations up to 1 μM. This study provides a new perspective for the construction of biosensors using nanozyme-mediated, highly stable, and efficient cascade signal amplification (Fig. 7g).

4.2. Disease therapy

In recent years, the application research of nanozymes in disease therapy has become increasingly in-depth, and their unique properties and broad application prospects have shown great potential in multiple disease fields. At present, their high POD-like activity has been explored in clinical anti-tumor, antibacterial, antiviral therapy and other fields.

4.2.1. Cancer therapy. Cancer has emerged as a major threat to human life and health. Traditional cancer treatments including surgery, radiotherapy, and chemotherapy often struggle to eradicate cancer, are associated with high side effects, and suffer from poor patient compliance. Consequently, it is important to identify novel and effective therapies that can supersede these traditional approaches. In recent years, the emergence of the field of nanozymes has ushered in new avenues for the development of therapeutic strategies that are responsive to the tumor microenvironment. Table 3 summarises the applications of nanozymes with POD-like activity in cancer therapy.

When nanozymes are applied to antitumor therapy, the overarching core mechanism involves the generation of ROS to eliminate tumor cells.[72] Among these, POD-like activity is the most frequently used for tumor therapy. For instance, Zeng *et al.* developed a brand-new peroxidase-mimetic nanozyme based on biodegradable boron nitride (BON) structure, which can *in vitro* and *in vivo* catalyze hydrogen peroxide to efficiently generate hydroxyl radicals.[149] Upon intratumoral injection, this material induced significant tumor cell apoptosis, demonstrating therapeutic efficacy comparable to that of anticancer drugs (Fig. 8a–f). Furthermore, Fan *et al.* developed nitrogen-doped porous carbon spheres for tumour catalytic therapy (Fig. 8g–m). In catalytic property assessment experiments, it was observed that these nitrogen-doped porous carbon spheres exhibited pH-dependent multi-enzyme activity. In acidic environments, they displayed POD-like and oxidase activities, tending to decompose H_2O_2 to generate toxic $^{\bullet}OH$ or convert O_2 to $^{\bullet}O^{2-}$. Conversely, under neutral conditions, they exhibited superoxide dismutase and catalase activities, decomposing and converting H_2O_2 and $^{\bullet}O^{2-}$, among

Table 3 Nanozymes with POD-like activity used for cancer therapy

Materials	Application	Target	Methods	Ref.
Ag@GQD	Cancer therapy	549, MCF-7	Synergistic therapy of chemotherapy drugs and nanozymes	138
IrO_x	Cancer therapy	A549 human lung adenocarcinoma	Mild photothermal-enhanced nanocatalysis therapy	139
SA-Rh	Cancer therapy	4T1 tumor-bearing BALB/c mice	By synergistic CDT and PTT modalities to Induce apoptosis in cancer cells	140
Ir–N_5 SA	Cancer therapy	Mouse breast cancer cells	Generate ROS	141
GQDs	Cancer therapy	A549 tumor	Deep tumor penetration of nanozymes in biomedical application	142
Cu–Ag	Cancer therapy	Mouse breast tumor cells	The production of $^{\bullet}OH$ induced by the Cu–Ag nanozyme triggered ferroptosis in tumor cells	143
Bi–NC	Cancer therapy	4T1 tumors	Catalyze the production of $^{\bullet}OH$ and depletes antioxidant GSH	144
FeO_x	Cancer therapy	4T1 cells	Catalyze the decomposition of H_2O_2 to O_2, allowing to alleviate the hypoxic environment of the tumors	145
Enzyme-MOF	Cancer therapy	Melanoma cells	Generate ROS and deplete GSH	146
Ir@$MnFe_2O_4$ NP	Cancer therapy	HeLa cells	Catalyze the conversion of H_2O_2 to cytotoxic $^{\bullet}OH$	147
FeSi	Cancer therapy	LM3 cells	Catalyze H_2O_2 into $^{\bullet}OH$	148

others, into non-toxic H_2O and O_2. This unique property renders nitrogen-doped porous carbon spheres a highly safe and efficient nano-enzymatic therapeutic agent. Upon accumulation at the tumor site, they generate toxic ROS using locally available O_2 and overexpressed H_2O_2, leading to significant tumor suppression and effectively prolonging survival in mice post-treatment.[48] In addition, the combination of nanomaterials and drugs is also promising in cancer treatment. Zhou group designed and constructed MOF-coated MnO_2 nanosheets to realize the co-delivery of a survivin inhibiting DNAzyme and doxorubicin for chemo-gene combinatorial treatment of cancer.[149] This strategy also paves the way for the future use of nanomaterials in disease treatment.

Besides, as treatment techniques continue to be optimized, the development of nanomaterials with synergistic tumor ablation has also gained considerable interest from researchers. For instance, Zhang *et al.* have developed pH-responsive Ce6-conjugated gold nanorods (Ce6-PEG-AuNRs), which can achieve fluorescence-guided PTT/PDT ablation of tumors.[150] Song *et al.* synthesized a Bi_2Se_3@HA-doped PPy/ZnPc nanodisc complex using bismuth as a raw material, which could simultaneously exert photothermal and photodynamic effects and had an excellent tumor-growth inhibition ratio (96.4%).[151] Liu *et al.* reported a novel Bi-based nanocomposite (UCNP@NBOF-FePc-PFA) that could not only enable the upconversion luminescence/CT bioimaging of

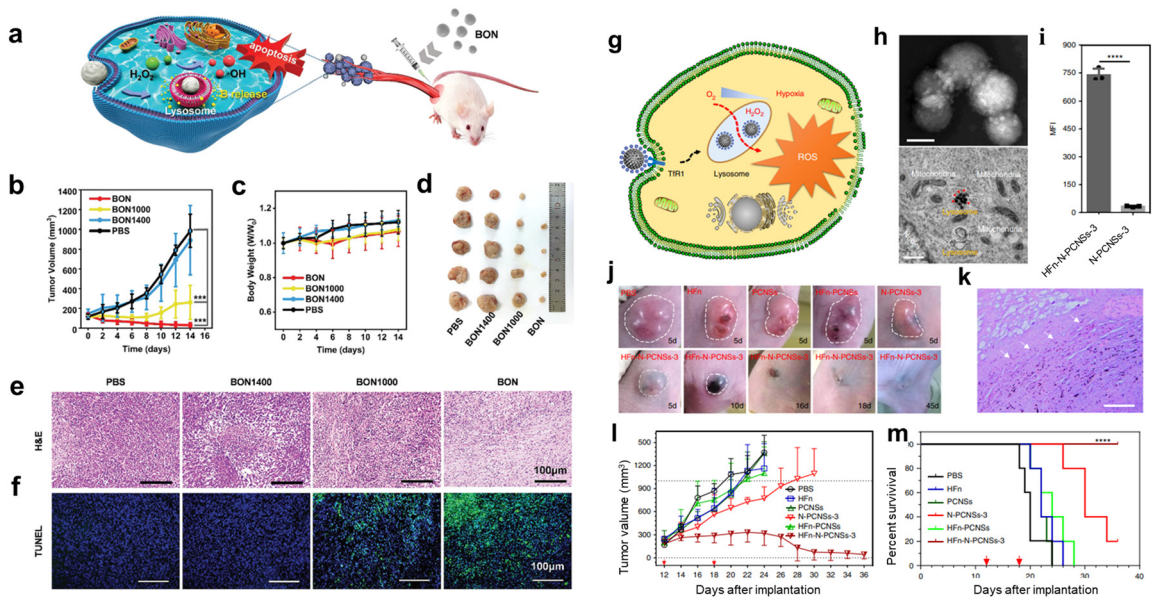

Fig. 8 *In vivo* evaluations of the BON nanozyme for breast cancer therapy. (a) Schematic of the therapeutic mechanism of BON. (b) Tumor growth curves of 4T1 tumors in BALB/c mice treated under different conditions. (c) Body weights of different groups of mice, (d) Photographs of exfoliated tumors of different groups. (e) Optical photographs of tumor sections stained with H&E. (f) Corresponding fluorescent images of tumor sections subjected to TUNEL staining. Adapted with permission.[149] Copyright 2021, Wiley. Tumor therapy based on N-PCNSs using HFn coordination. (g) Schematic of N-PCNS-induced tumor cell destruction *via* ferritin-mediated specific delivery. (h) TEM image of HFn assembled onto N-PCNSs and TEM image of cancer cells treated with HFn-PCNSs. (i) Quantification of HFn-enhanced internalization of N-PCNSs by flow cytometry analysis. (j) Photographs of tumors after treatment in different groups. (k) Enrichment of the material at the tumor site. (l) Changes in the tumor volume during treatment in different groups. (m) Evaluation of the survival rate in mice. Adapted with permission.[48] Copyright 2021, Nature portfolio.

living beings but also be applied for photothermal/photodynamic/radio synergistic tumor ablation.[152] These materials have great antitumor effects and potential applications in biomedicine. Luo group prepared silver-modified polyvinyl alcohol pyrrolidone nanoparticles with nano-heterostructures by a two-step method (Bi–Ag@PVP NPs).[153] After modification of PVP, the Bi–Ag@PVP NPs possessed low cytotoxicity and caused little damage to normal organs. Notably, under 808 nm laser irradiation, the Bi–Ag@PVP NPs exhibited a better photothermal effect than single bismuth NPs (Bi@PVP NPs) *in vivo* and *in vitro*. Importantly, the Bi–Ag@PVP NPs could employ NIR to generate ROS, thereby synergizing PDT and PTT to ablate tumor cells, achieving an enhanced therapeutic effect. Meanwhile, the BiAg@PVP NPs also possessed computed tomography (CT) and photoacoustic (PA) dual-modal imaging properties, enhancing the CT and PA contrast of tumor sites. Interestingly, the Bi–Ag@PVP NPs could be effectively used to kill *Escherichia coli*, indicating that the Bi–Ag@PVP NPs had an excellent antibacterial function and could be used to avoid bacterial infections during cancer therapy.

4.2.2. Antibacterial therapy. In recent years, excessive use of antibiotics has resulted in a large number of multidrug-resistant bacteria, which has had a serious impact on public health. The existence of multidrug-resistant bacteria significantly limits the drug options available for patients with bacterial infections, and in some cases, leaves them without effective treatment. Nanozyme antibacterial therapy is a new antibacterial therapy after photodynamic antibacterial therapy. The emergence of nanozyme antibacterial therapy provides a new means to resist multidrug-resistant bacteria. Table 4 summarises the applications of nanozymes with POD-like activity in antibacterial therapy. Nanozyme exhibiting POD-like activity can catalyze the production or consumption of ROS. Excessive reactive oxygen radicals can damage cell membranes, proteins and nucleic acids, and kill pathogenic microorganisms, including bacteria and fungi. In recent years, nanozymes have shown promising applications in antimicrobial therapy. Pan *et al.* designed Au^{3+}-functionalized UIO-67 MOF nanoparticles as mimics of POD and oxidase double enzymes, which catalyze H_2O_2 and oxygen to generate $^{\bullet}OH$ and $^{\bullet}O^{2-}$ to kill *Escherichia coli* and *Staphylococcus aureus* and promote wound healing (Fig. 9a–e).

At the same time, because metal ions from metals and oxides can be toxic, how to cut down the amount of metals is another important issue. Therefore, SAzymes have gradually been developed for antibacterial therapy in recent years.

Compared with traditional nanozymes, SAzymes have the advantages of high atomic utilization efficiency and high catalytic activity. Fan *et al.* loaded single-atom Pt on graphitized carbon nitride (SA-Pt/g–C_3N_4–K) and constructed an efficient single-atom peroxidase mimic.[166] Theoretical calculations showed that SA-Pt/g–C_3N_4–K with a Pt–N–C structure significantly increased the production of $^{\bullet}OH$ by reducing the desorption energy of OH* active intermediate at the active site during H_2O_2 activation. In the mouse wound model infected by *Escherichia coli*, SA-Pt/g–C_3N_4–K + H_2O_2 group effectively promoted wound healing in the past 6 days, and compared with the other groups, SA-Pt/g–C_3N_4–K + H_2O_2 group had optimal healing efficiency (Fig. 9f–j).

In addition, nanozyme-catalyzed therapy combined with PTT is a promising approach. Cheng group prepared a pyrolytic-etch-adsorption-pyrolysis (PEAP) process that can be used as a photothermal catalytic antibacterial nanozyme (Cu SASs/NPC). Compared with undoped Cu NPCS, Cu SASs/NPCS have stronger catalytic activity, GSH consumption and photothermal effect.[167] The prepared Cu SASs/NPC can be used as peroxidase nanase to catalyze H_2O_2 to generate $^{\bullet}OH$ efficiently, thus achieving obvious bactericidal effects. The photothermal effect of Cu SASs/NPC under laser irradiation can further improve the catalytic action of peroxide-like enzymes, thus producing more ROS and achieving better antibacterial effects *in vitro*. More importantly, Cu SASs/NPC effectively eradicates internal bacterial infections transmitted by MRSA pathogens at the wound site, resulting in better internal wound healing. The application of SAzymes in the biomedical field is further expanded.

Nanozymes with photothermal and photodynamic properties have also been reported. Yang group designed and synthesized a

Table 4 Nanozymes with POD-like activity used for antibacterial therapy

Materials	Application	Target	Methods	Ref.
Fe@HCMS	Antibacterial therapy	Gram-positive *S. aureus* and Gram-negative *E. coli*	ROS mediated biocatalytic therapy	154
Au@$Cu_{2-x}S$	Antibacterial therapy	Gram-positive *Enterococcus faecalis* and Gram-negative *Fusobacterium*	Synergistic antimicrobial system	155
CuTAQ	Antibacterial therapy	*S. aureus*, *E. coli*	Metal-polyphenol nanomaterials in efficient antimicrobial	156
$CuCo_2O_4$	Antibacterial therapy	*E. coli*	Generate $^{\bullet}OH$ and $^{\bullet}O^{2-}$	157
Fe_3O_4	Antibacterial therapy	*S. aureus*	To catalyze the production of more $^{\bullet}OH$ for killing bacteria	158
Cu_2O/Pt	Antibacterial therapy	Gram-positive *S. aureus* and Gram-negative *E. coli*	Photothermal properties of the Cu_2O/Pt nanozyme for enhanced CDT	159
Fe–N–C SAzyme	Antibacterial therapy	*E. coli* and *S. aureus*	Spherical mesoporous SAzymes as an antibiotic	160
Fe_3O_4@MOF@Au NPs	Antibacterial therapy	Gram-positive *S. aureus* and Gram-negative *E. coli*	Generate $^{\bullet}OH$	161
Fe-CDs	Antibacterial therapy	Gram-positive and Gram-negative bacteria	Carbon dots as the antibiotics-free nano platforms	162
VO_xC NSs	Antibacterial therapy	*E. coli* and *S. aureus*	Generate hydroxyl radicals for bacterial killing	163
Cu SASs/NPC	Antibacterial therapy	*E. coli*, *S. aureus*	Antibacterial and anti-infective bio-applications of Cu single-atom-containing catalysts	164

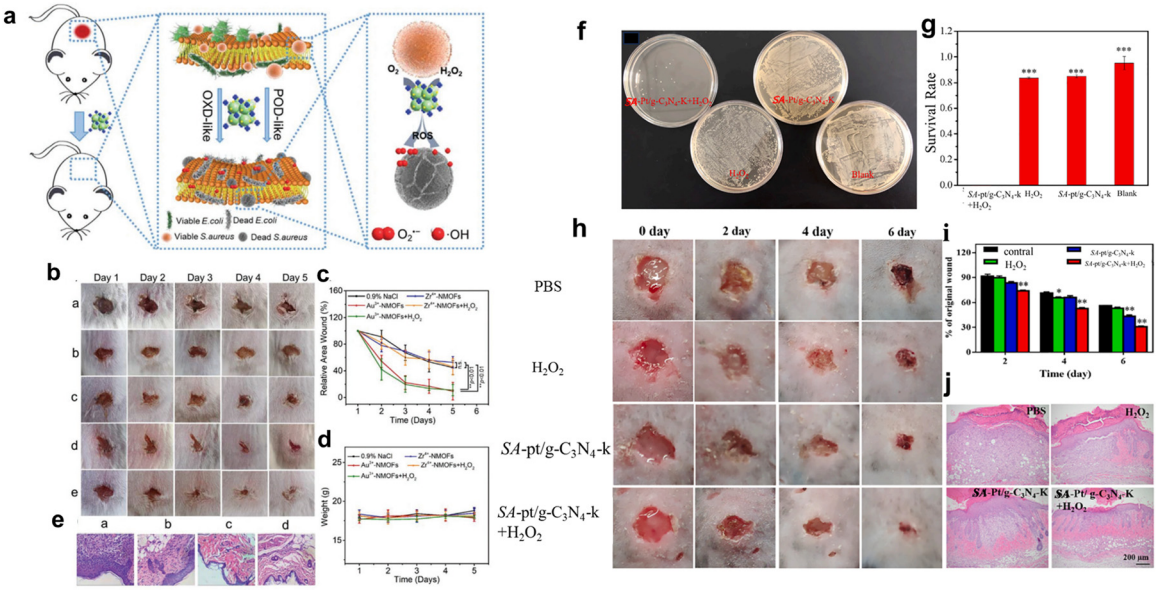

Fig. 9 (a) Use of Au^{3+}-NMOFs as nanozymes for antibacterial therapy. (b)–(e) Probing the wound-healing efficiencies and cytotoxicity of the Au^{3+}-NMOFs and control systems. Adapted with permission.[165] Copyright 2022, Wiley. (f) Comparison of the catalytic activity of different materials. (g) ESR demonstrating the generation of •OH. (h) Wound photographs of different treatment groups at different days and (i) corresponding wound diameter size. (j) H&E staining of wounds in different groups at the end of treatment. Adapted with permission.[166] Copyright 2022, Elsevier.

nanozyme CeO_2/FePPOP composite of a porphyrin-based porous organic polymer, FePPOP, and an inorganic material, CeO_2, for multimodal antimicrobial activity.[168] By subjecting CeO_2/FePPOP to a single near-infrared (NIR) light, it is possible to catalyze the production of a significant amount of ROS. This material also has excellent light-to-heat conversion efficiency, thereby inflicting dual damage on bacteria. It provides innovative insights for the creation of nanomaterial antimicrobials suitable for phototherapy interventions.

4.2.3. Antiviral therapy. At present, the strategies to combat viral diseases are prevention (vaccine) and treatment (antiviral drugs and antibodies). However, drug resistance caused by high mutations in the viral genome is a major challenge in the development of antiviral drugs. For this reason, nanozymes use their catalytic and physicochemical properties to directly or indirectly inactivate viruses, providing a new direction for the fight against viral infection. The role of nanozymes in virus therapy primarily involves increasing ROS levels, regulating the immune environment, inhibiting virus replication, and oxidizing viral lipid envelopes and proteins. For the new coronavirus (SARS-CoV2) which is still prevalent at present, Wang *et al.* Successfully designed a single-atom silver

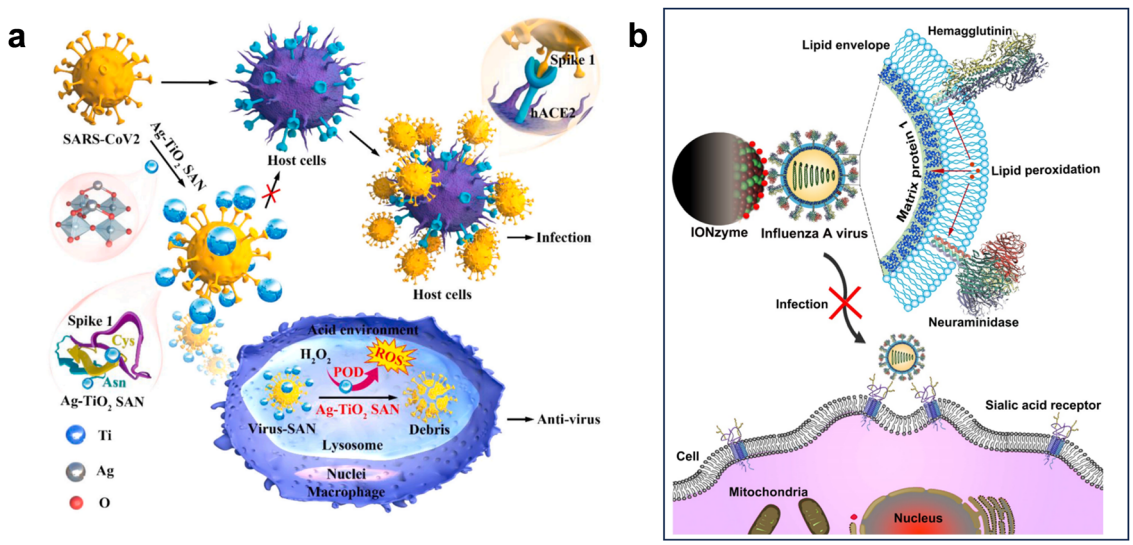

Fig. 10 (a) Schematic of Ag–TiO_2 against SARS-CoV2 virus. Adapted with permission.[169] Copyright 2021, Elsevier. (b) Schematic of the Fe_3O_4 nanozyme against influenza virus. Adapted with permission.[170] Copyright 2019, Spring International Publisher.

nanozyme (Ag–TiO_2) with titanium dioxide as the carrier, and proved that the SAzyme has good potential anti-SARS-CoV2 activity.[169]

The new SAzyme showed strong adsorption ability to SARS-CoV2 pseudovirus *in vitro*, and the adsorption rate was as high as 99.65%. The pseudovirus highly expressed SARS-CoV2 spike protein on the surface of HIV-1. Theoretical calculations and experimental evidence indicate that the Ag atom in Ag–TiO_2 is strongly bound to cysteine and asparagine, which are the most abundant amino acids on the surface of the spike protein. *In vivo*, the nanozymes can effectively facilitate the phagocytosis of virus by macrophages. The intrinsic POD-like activity of Ag–TiO_2 exhibited a potent antiviral effect within lysosomes. Through the virus elimination model, it was found that Ag–TiO_2 could significantly eliminate SARS-CoV2 pseudoviruses and protect host cells from infection (Fig. 10a). In addition, the influenza virus is a very widespread virus. Based on this, Qin *et al.* reported a strategy using nanozymes against influenza virus.[170] Influenza A viruses (IAVs) are characterized by a granular shape with a diameter of 80–120 nm, which is composed of segmented RNA and glycoprotein. In the process of action, the Fe_3O_4 nanozyme directly contacts IAV particles and collapses their lipid envelopes by elevating lipid peroxidation levels. This, in turn, generates free radicals that damage adjacent proteins such as hemagglutinin, neuraminidase, and matrix protein 1, ultimately impairing the structure and function of the viruses and preventing their infection of host cells (Fig. 10b).

5. Conclusion and prospects

The advances in nanotechnology offer huge opportunities for the development of POD-like nanomaterials. Some specific breakthroughs have allowed various strategies to give nanomaterial POD-like activity. With the unique advantages of low cost, high stability and easy preparation, POD-like nanozymes have already become effective substitutes for natural enzymes. This review provided an overview of the classification and activity regulation strategy of POD-like nanozymes. Furthermore, we comprehensively reviewed the latest advances in nanomaterials with POD-like activity in biosensing and disease treatment.

Although breakthroughs have been accomplished in the research of POD-like nanozymes, their development still faces challenges: (1) the catalytic mechanism and key catalytic sites of nanozymes need to be analyzed in depth. At present, most of the research on nanozymes focuses on the optimization of catalytic activity, but less on the analysis of catalytic mechanisms. Although some studies have used advanced mathematical methods such as quantum mechanical computational simulation, molecular dynamics simulation, and machine learning to predict the catalytic pathways of nanozymes, few studies have been able to clarify the key sites of nanozymes that are playing the main catalytic role. Furthermore, little attention has been paid to understanding the dynamic changes in the nanozyme structure during catalysis through experimental verification. Therefore, it is of great importance to employ advanced characterization methods, which can not only help us deeply analyze the catalytic mechanism of nanozymes but also understand the entire process of catalytic reactions from the atomic/molecular level. (2) Catalytic activity and specificity of nanozymes. Generally speaking, the catalytic activity of nanozymes is derived from the active site located on the surface, which means that the more exposed the surface, the higher the catalytic activity. However, excessive exposure will lead to the lack of surface modification of nanozymes and reduce their stability. Additionally, nanozymes are inherently nonspecific. Nonetheless, research has demonstrated that nanozymes can be specific by surface modification of antibodies, nucleic acids, small molecules, and some structural polymers. Nevertheless, most of the surface modifications also weaken the catalytic activity of nanozymes. Thus, the balance between catalytic activity and specificity, as well as the choice of surface modification, remains yet to be studied. (3) The biosafety of nanozymes needs to be further explored. Furthermore, similar to other nanomaterials, toxicological studies of nanozymes including long-term cytotoxicity, administration routes, metabolism processes, excretion mechanisms, biodistribution patterns, pharmacokinetics, pharmacodynamics in large animals, and *in vivo* experiments, remain largely unproven. Furthermore, the targeting, specificity, *in vivo* activity and localization of nanozymes are still unclear for catalytic therapeutic effects. Given the complexity of the *in vivo* microenvironment, the catalytic pathways of nanozymes often become uncontrollable. At the same time, the mechanisms of potential in *in vivo* biocatalytic reactions and biological interfaces are also difficult to predict, all of which will be factors affecting biosecurity. Therefore, systematic studies and analyses are needed on the *in vivo* stability, pharmacokinetics (such as uptake, distribution, and metabolism), duration of therapeutic effects, and toxicity (including hemolysis and coagulation analysis) of nanozymes. (4) Strengthen interdisciplinary integration. We believe that the future of POD-like nanomaterials requires interdisciplinary collaboration, including chemistry, physics, biology, and materials science. Furthermore, devices derived from 3D-printed POD-like nanomaterials, especially biosensors, hold the promise of meeting the portability and functional needs of biomedical applications. However, it is acknowledged that numerous existing applications of high-performance POD nanomaterials are still at the proof-of-concept stage, having only been demonstrated in laboratory environments. We believe that there is still a long way to go before commercial applications. The long-term stability and durability of POD-like nanomaterial systems need to be verified prior to practical application. Through the efforts of these different research areas, POD-like nanomaterials can provide more opportunities for personalized disease diagnosis, high-precision bioimaging, biosensing, and drug delivery. In summary, we anticipate that addressing these unresolved issues will significantly contribute to expanding the applications of POD-like nanozymes.

Data availability

Data availability is not applicable to this article as no new data were created or analysed in this study.

Conflicts of interest

The authors declare that they have no known competing financial interests or personal relationships that could have appeared to influence the work reported in this paper.

Acknowledgements

This research was funded by the National Natural Science Foundation of China (No. 82102466, 82102466, 81871713 and 82003262), the National Organ Transplantation Special Support Project (No. 2019JYJH08), the Key Research and Development Project of Technology Department of Sichuan Province (No. 2023YFS0108, 2021YFS0160 and 2020YFS0228), and the 1·3·5 Incubation Project of West China Hospital of Sichuan University (No. 19HXFH023).

References

1 X. Lian, Y. Fang, E. Joseph, Q. Wang, J. Li, S. Banerjee, C. Lollar, X. Wang and H.-C. Zhou, *Chem. Soc. Rev.*, 2017, **46**, 3386–3401.
2 J. Wu, X. Wang, Q. Wang, Z. Lou, S. Li, Y. Zhu, L. Qin and H. Wei, *Chem. Soc. Rev.*, 2019, **48**, 1004–1076.
3 L. Gao, J. Zhuang, L. Nie, J. Zhang, Y. Zhang, N. Gu, T. Wang, J. Feng, D. Yang, S. Perrett and X. Yan, *Nat. Nanotechnol.*, 2007, **2**, 577–583.
4 J. Shah, A. Pandya, P. Goyal, S. K. Misra and S. Singh, *ACS Appl. Energy Mater.*, 2020, **3**, 3355–3370.
5 D. Yang, Q. Li, S. K. Tammina, Z. Gao and Y. Yang, *Sens. Actuators, B*, 2020, **319**, 128273.
6 X. Wu, T. Chen, Y. Chen and G. Yang, *J. Mater. Chem. B*, 2020, **8**, 2650–2659.
7 R. Das, A. Dhiman, A. Kapil, V. Bansal and T. K. Sharma, *Anal. Bioanal. Chem.*, 2019, **411**, 1229–1238.
8 W. He, X. Han, H. Jia, J. Cai, Y. Zhou and Z. Zheng, *Sci. Rep.*, 2017, **7**, 7.
9 U. Jain, S. Gupta and N. Chauhan, *Int. J. Biol. Macromol.*, 2017, **105**, 549–555.
10 J. Yang, J. Y. Lee and H. P. Too, *J. Phys. Chem. B*, 2005, **109**, 19208.
11 C. Ge, G. Fang, X. Shen, Y. Chong, W. G. Wamer, X. Gao, Z. Chai, C. Chen and J.-J. Yin, *ACS Nano*, 2016, **10**, 10436–10445.
12 X. Yuan, S. Cheng, L. Chen, Z. Cheng, J. Liu, H. Zhang, J. Yang and Y. Li, *Talanta*, 2023, **258**, 124407.
13 X. He, J. Li, R. Li, D. Zhao, L. Zhang, X. Ji, X. Fan, J. Chen, Y. Wang, Y. Luo, D. Zheng, L. Xie, S. Sun, Z. Cai, Q. Liu, K. Ma and X. Sun, *Inorg. Chem.*, 2022, **62**, 25–29.
14 N. N. Nghia, B. T. Huy and Y.-I. Lee, *Microchim. Acta*, 2018, **186**, 1.
15 R. Li, X. Qiao, H. Ma, H. Li, C. Li and L. Jin, *J. Mater. Chem. B*, 2022, **10**, 3311–3319.
16 M. A. Wahab, S. M. A. Hossain, M. K. Masud, H. Park, A. Ashok, M. Mustapić, M. Kim, D. Patel, M. Shahbazi, M. S. A. Hossain, Y. Yamauchi and Y. V. Kaneti, *Sens. Actuators, B*, 2022, **366**, 131980.
17 Z. Lou, S. Zhao, Q. Wang and H. Wei, *Anal. Chem.*, 2019, **91**, 15267–15274.
18 M. Li, J. Chen, W. Wu, Y. Fang and S. Dong, *J. Am. Chem. Soc.*, 2020, **142**, 15569–15574.
19 T. Zhang, Y. Xing, Y. Song, Y. Gu, X. Yan, N. Lu, H. Liu, Z. Xu, H. Xu, Z. Zhang and M. Yang, *Anal. Chem.*, 2019, **91**, 10589–10595.
20 M. Wang, X. Zhou, Y. Li, Y. Dong, J. Meng, S. Zhang, L. Xia, Z. He, L. Ren, Z. Chen and X. Zhang, *Bioact. Mater.*, 2022, **17**, 289–299.
21 L. Huang, J. Chen, L. Gan, J. Wang and S. Dong, *Sci. Adv.*, 2019, **5**, eaav5490.
22 R. Das, A. Dhiman, A. Kapil, V. Bansal and T. K. Sharma, *Anal. Bioanal. Chem.*, 2019, **411**, 1229–1238.
23 S. Cai, C. Qi, Y. Li, Q. Han, R. Yang and C. Wang, *J. Mater. Chem. B*, 2016, **4**, 1869–1877.
24 Q. Wang, L. Zhang, C. Shang, Z. Zhang and S. Dong, *Chem. Commun.*, 2016, **52**, 5410–5413.
25 R. Pan, G. Li, S. Liu, X. Zhang, J. Liu, Z. Su and Y. Wu, *Trends Anal. Chem.*, 2021, **145**, 1164642.
26 Z. Yang, Y. Cao, J. Li, M. Lu, Z. Jiang and X. Hu, *ACS Appl. Mater. Interfaces*, 2016, **8**, 12031–12038.
27 C. Huang, F. Zhang, Q. Wang, Y. Lin and J. Huang, *Anal. Methods*, 2020, **12**, 1988–1994.
28 Y. Yue, H. Wei, J. Guo and Y. Yang, *Colloids Surf., A*, 2021, **610**, 127515.
29 Z. Fu, W. Zeng, S. Cai, H. Li, J. Ding, C. Wang, Y. Chen, N. Han and R. Yang, *J. Colloid Interface Sci.*, 2021, **604**, 113–121.
30 L. Li, H. Liu, J. Bian, X. Zhang, Y. Fu, Z. Li, S. Wei, Z. Xu, X. Liu, Z. Liu, D. Wang and D. Gao, *Chem. Eng. J.*, 2020, **397**, 125438.
31 C. Wei, Y. Liu, X. Zhu, X. Chen, Y. Zhou, G. Yuan, Y. Gong and J. Liu, *Biomaterials*, 2020, **238**, 119848.
32 Z. Chen, T. Zhang, Y. Liu, X. Zhang, L. Chen, Z. Zhang and N. Lu, *ACS Appl. Nano Mater.*, 2024, **7**, 3645–3655.
33 R. André, F. Natálio, M. Humanes, J. Leppin, K. Heinze, R. Wever, H. C. Schröder, W. E. G. Müller and W. Tremel, *Adv. Funct. Mater.*, 2010, **21**, 501–509.
34 S. Yao, X. Zhao, X. Wang, T. Huang, Y. Ding, J. Zhang, Z. Zhang, Z. L. Wang and L. Li, *Adv. Mater.*, 2022, **34**, 2109568.
35 D. Feng, Z. Y. Gu, J. R. Li, H. L. Jiang, Z. Wei and H. C. Zhou, *Angew. Chem., Int. Ed.*, 2012, **51**, 10307–10310.
36 T. Zhang, Y. Xing, Y. Song, Y. Gu, X. Yan, N. Lu, H. Liu, Z. Xu, H. Xu, Z. Zhang and M. Yang, *Anal. Chem.*, 2019, **91**, 10589–10595.
37 S. Ji, B. Jiang, H. Hao, Y. Chen, J. Dong, Y. Mao, Z. Zhang, R. Gao, W. Chen, R. Zhang, Q. Liang, H. Li, S. Liu, Y. Wang, Q. Zhang, L. Gu, D. Duan, M. Liang, D. Wang, X. Yan and Y. Li, *Nat. Catal.*, 2021, **4**, 407–417.
38 N. Alizadeh and A. Salimi, *J. Nanobiotechnol.*, 2021, **19**, 26.
39 D. Liu, C. Ju, C. Han, R. Shi, X. Chen, D. Duan, J. Yan and X. Yan, *Biosens. Bioelectron.*, 2021, **173**, 112817.

40 Z. Xu, Z. Qiu, Q. Liu, Y. Huang, D. Li, X. Shen, K. Fan, J. Xi, Y. Gu, Y. Tang, J. Jiang, J. Xu, J. He, X. Gao, Y. Liu, H. Koo, X. Yan and L. Gao, *Nat. Commun.*, 2018, **9**, 3713.
41 D. Li, Q. Guo, L. Ding, W. Zhang, L. Cheng, Y. Wang, Z. Xu, H. Wang and L. Gao, *ChemBioChem*, 2020, **21**, 2620–2627.
42 H. Ding, B. Hu, B. Zhang, H. Zhang, X. Yan, G. Nie and M. Liang, *Nano Res.*, 2020, **14**, 570–583.
43 W. Ma, Y. Xue, S. Guo, Y. Jiang, F. Wu, P. Yu and L. Mao, *Chem. Commun.*, 2020, **56**, 5115–5118.
44 Y. Song, K. Qu, C. Zhao, J. Ren and X. Qu, *Adv. Mater.*, 2010, **22**, 2206–2210.
45 Y. Song, X. Wang, C. Zhao, K. Qu, J. Ren and X. Qu, *Chem. – Eur. J.*, 2010, **16**, 3617–3621.
46 Y. Hu, X. J. Gao, Y. Zhu, F. Muhammad, S. Tan, W. Cao, S. Lin, Z. Jin, X. Gao and H. Wei, *Chem. Mater.*, 2018, **30**, 6431–6439.
47 Z. Lou, S. Zhao, Q. Wang and H. Wei, *Anal. Chem.*, 2019, **91**, 15267–15274.
48 K. Fan, J. Xi, L. Fan, P. Wang, C. Zhu, Y. Tang, X. Xu, M. Liang, B. Jiang, X. Yan and L. Gao, *Nat. Commun.*, 2018, **9**, 1440.
49 Q. Wang and D. Astruc, *Chem. Rev.*, 2019, **120**, 1438–1511.
50 D. Ni, J. Lin, N. Zhang, S. Li, Y. Xue, Z. Wang, Q. Liu, K. Liu, H. Zhang, Y. Zhao, C. Chen and Y. Liu, *Wiley Nanomed. Nanobiotechnol.*, 2022, **14**, 1773.
51 M. Wang, X. Zhou, Y. Li, Y. Dong, J. Meng, S. Zhang, L. Xia, Z. He, L. Ren, Z. Chen and X. Zhang, *Bioact. Mater.*, 2022, **17**, 289–299.
52 Y. Lu, J. Li, Y. Liu, L. Zhu, S. Xiao, M. Bai, D. Chen and T. Xie, *Microchim. Acta*, 2023, **190**, 71.
53 C. Zhao, X. Tang, J. Zhao, J. Cao, Z. Jiang and J. Qin, *J. Nanobiotechnol.*, 2022, **20**, 507.
54 B. Jiang and M. Liang, *Chin. J. Chem.*, 2020, **39**, 174–180.
55 Q. Chen, S. Li, Y. Liu, X. Zhang, Y. Tang, H. Chai and Y. Huang, *Sens. Actuators, B*, 2020, **305**, 127511.
56 B. Xu, H. Wang, W. Wang, L. Gao, S. Li, X. Pan, H. Wang, H. Yang, X. Meng, Q. Wu, L. Zheng, S. Chen, X. Shi, K. Fan, X. Yan and H. Liu, *Angew. Chem., Int. Ed.*, 2019, **58**, 4911–4916.
57 S. Lin and H. Wei, *Sci. China: Life Sci.*, 2019, **62**, 710–712.
58 Y. Wang, G. Jia, X. Cui, X. Zhao, Q. Zhang, L. Gu, L. Zheng, L. H. Li, Q. Wu, D. J. Singh, D. Matsumura, T. Tsuji, Y.-T. Cui, J. Zhao and W. Zheng, *Chem*, 2021, **7**, 436–449.
59 X. Wang, L. Qin, M. Zhou, Z. Lou and H. Wei, *Anal. Chem.*, 2018, **90**, 11696–11702.
60 M. N. Ivanova, E. D. Grayfer, E. E. Plotnikova, L. S. Kibis, G. Darabdhara, P. K. Boruah, M. R. Das and V. E. Fedorov, *ACS Appl. Mater. Interfaces*, 2019, **11**, 22102–22112.
61 Z. Li, X. Yang, Y. Yang, Y. Tan, Y. He, M. Liu, X. Liu and Q. Yuan, *Chem. Eur. J.*, 2017, **24**, 409–415.
62 X. Xia, J. Zhang, N. Lu, M. J. Kim, K. Ghale, Y. Xu, E. McKenzie, J. Liu and H. Ye, *ACS Nano*, 2015, **9**, 9994–10004.
63 F. F. Peng, Y. Zhang and N. Gu, *Chin. Chem. Lett.*, 2008, **19**, 730–733.
64 S. R. Ahmed, K. Takemeura, T.-C. Li, N. Kitamoto, T. Tanaka, T. Suzuki and E. Y. Park, *Biosens. Bioelectron.*, 2017, **87**, 558–565.
65 M. S. Kim, S. Cho, S. H. Joo, J. Lee, S. K. Kwak, M. I. Kim and J. Lee, *ACS Nano*, 2019, **13**, 4312–4321.
66 Q. Liang, J. Xi, X. J. Gao, R. Zhang, Y. Yang, X. Gao, X. Yan, L. Gao and K. Fan, *Nano Today*, 2020, **35**, 100935.
67 Y. Zhu, J. Wu, L. Han, X. Wang, W. Li, H. Guo and H. Wei, *Anal. Chem.*, 2020, **92**, 7444–7452.
68 W. Guo, M. Zhang, Z. Lou, M. Zhou, P. Wang and H. Wei, *ChemCatChem*, 2018, **11**, 737–743.
69 Z. Xi, W. Gao and X. Xia, *ChemBioChem*, 2020, **21**, 2440–2444.
70 Y. Fu, X. Zhao, J. Zhang and W. Li, *J. Phys. Chem. C*, 2014, **118**, 18116–18125.
71 S. Liu, F. Lu, R. Xing and J. J. Zhu, *Chem. – Eur. J.*, 2010, **17**, 620–625.
72 J. Yang, H. Yao, Y. Guo, B. Yang and J. Shi, *Angew. Chem., Int. Ed.*, 2022, **61**, 202200480.
73 C. Ge, R. Wu, Y. Chong, G. Fang, X. Jiang, Y. Pan, C. Chen and J. J. Yin, *Adv. Funct. Mater.*, 2018, **28**, 1801484.
74 J. Li, W. Liu, X. Wu and X. Gao, *Biomaterials*, 2015, **48**, 37–44.
75 J. Huo, J. Hao, J. Mu and Y. Wang, *ACS Appl. Bio Mater.*, 2021, **4**, 3443–3452.
76 X. Fan, B. Cai, R. Du, R. Hübner, M. Georgi, G. Jiang, L. Li, M. Samadi Khoshkhoo, H. Sun and A. Eychmüller, *Chem. Mater.*, 2019, **31**, 10094–10099.
77 B. Liu and J. Liu, *Nanoscale*, 2015, **7**, 13831–13835.
78 X. Wang, W. Cao, L. Qin, T. Lin, W. Chen, S. Lin, J. Yao, X. Zhao, M. Zhou, C. Hang and H. Wei, *Theranostics*, 2017, **7**, 2277–2286.
79 J. Shah, R. Purohit, R. Singh, A. S. Karakoti and S. Singh, *J. Colloid Interface Sci.*, 2015, **456**, 100–107.
80 N. V. S. Vallabani, A. S. Karakoti and S. Singh, *Colloids Surf., B*, 2017, **153**, 52–60.
81 S. Bhagat and S. Singh, *Adv. Funct. Mater.*, 2024, **34**, 2408043.
82 L. Rastogi, D. Karunasagar, R. B. Sashidhar and A. Giri, *Sens. Actuators, B*, 2017, **240**, 1182–1188.
83 H. Sun, A. Zhao, N. Gao, K. Li, J. Ren and X. Qu, *Angew. Chem., Int. Ed.*, 2015, **54**, 7176–7180.
84 J. Tian, Q. Liu, A. M. Asiri, A. H. Qusti, A. O. Al-Youbi and X. Sun, *Nanoscale*, 2013, **5**, 11604–11609.
85 L. Huang, Q. Zhu, J. Zhu, L. Luo, S. Pu, W. Zhang, W. Zhu, J. Sun and J. Wang, *Inorg. Chem.*, 2019, **58**, 1638–1646.
86 H.-Q. Zheng, C.-Y. Liu, X.-Y. Zeng, J. Chen, J. Lü, R.-G. Lin, R. Cao, Z.-J. Lin and J.-W. Su, *Inorg. Chem.*, 2018, **57**, 9096–9104.
87 M. Zhao, Y. Li, X. Ma, M. Xia and Y. Zhang, *Talanta*, 2019, **200**, 293–299.
88 T. Zhang, S. Zhu, J. Wang, Z. Liu, M. Wang, S. Li and Q. Huang, *Spectrochim. Acta, Part A*, 2023, **291**, 122307.
89 X. Qu, J. Zou, Y. Shen, B. Zhao, J. Liang, Z. Wang, Y. Zhang and L. Niu, *Analyst*, 2022, **147**, 1808–1814.
90 H. Zhu, Y. Cai, A. Qileng, Z. Quan, W. Zeng, K. He and Y. Liu, *J. Hazard. Mater.*, 2021, **411**, 125090.
91 R. Zhu, W. Huang, X. Ma, Y. Zhang, C. Yue, W. Fang, Y. Hu, J. Wang, J. Dang, H. Zhao and Z. Li, *Anal. Chim. Acta*, 2019, **1089**, 131–143.

92 Z. Zhu, X. Lin, L. Wu, C. Zhao, Y. Zheng, A. Liu, L. Lin and X. Lin, *Sens. Actuators, B*, 2018, **274**, 609–615.
93 D. Gogoi, C. Hazarika, G. Neog, P. Mridha, H. K. Bora, M. R. Das, S. Szunerits and R. Boukherroub, *ACS Appl. Mater. Interfaces*, 2024, **16**, 14645–14660.
94 L. Su, Y. Cai, L. Wang, W. Dong, G. Mao, Y. Li, M. Zhao, Y. Ma and H. Zhang, *Microchim. Acta*, 2020, **187**, 132.
95 G. Yue, S. Li, W. Liu, F. Ding, P. Zou, X. Wang, Q. Zhao and H. Rao, *Sens. Actuators, B*, 2019, **287**, 408–415.
96 M.-Y. Shi, M. Xu and Z.-Y. Gu, *Anal. Chim. Acta*, 2019, **1079**, 164–170.
97 S. Dong, Y. Dong, T. Jia, S. Liu, J. Liu, D. Yang, F. He, S. Gai, P. Yang and J. Lin, *Adv. Mater.*, 2020, **32**, 2002439.
98 M. I. Halawa, Q. Xia and B. S. Li, *J. Mater. Chem. B*, 2021, **9**, 8038–8047.
99 M. Tian, L. Zhao, Y. Wang, G. Liu and P. Zhang, *Anal. Lett.*, 2022, **56**, 643–655.
100 X. Huang and J. Ren, *Anal. Chim. Acta*, 2011, **686**, 115–120.
101 Y. Pei, L. Zeng, C. Wen, K. Wu, A. Deng and J. Li, *Microchim. Acta*, 2021, **188**, 194.
102 Z. Dong, S. Xia, A. A. M. A. Alboull, I. M. Mostafa, A. Abdussalam, W. Zhang, S. Han and G. Xu, *ACS Appl. Nano Mater.*, 2024, **7**, 2983–2991.
103 Q. Xu, J. Li, S. Li and H. Pan, *J. Solid State Electrochem.*, 2012, **16**, 2891–2898.
104 Z.-M. Zhou, Y. Yu and Y.-D. Zhao, *Analyst*, 2012, **137**, 4262–4266.
105 X. Zeng, H. Liu, K. Wu, A. Deng and J. Li, *Analyst*, 2022, **147**, 1321–1328.
106 Y. Lin, Y. Sun, Y. Dai, W. Sun, X. Zhu, H. Liu, R. Han, D. Gao, C. Luo and X. Wang, *Talanta*, 2020, **207**, 120300.
107 J. Li, Y. Li, K. Wu, A. Deng and J. Li, *Talanta*, 2023, **265**, 124870.
108 S. Luo, J. Gao, J. Xian, H. Ouyang, L. Wang and Z. Fu, *Anal. Chem.*, 2022, **94**, 13533–13539.
109 Y. Liu, H. Ma, J. Gao, D. Wu, X. Ren, T. Yan, X. Pang and Q. Wei, *Biosens. Bioelectron.*, 2016, **79**, 71–78.
110 Z.-Y. Wang, Z.-Y. Tsai, H.-W. Chang and Y.-C. Tsai, *Micromachines*, 2024, **15**, 105.
111 S. Farokhi, M. Roushani and H. Hosseini, *Electrochim. Acta*, 2020, **362**, 137218.
112 R. Tang, S. Wang, H. Shao, S. Yang, Q. Liu, X. Chen, Y. Huang, N. Gan and S. Huang, *Sens. Actuators, B*, 2024, **410**, 137514.
113 T. Feng, X. Qiao, H. Wang, Z. Sun and C. Hong, *Biosens. Bioelectron.*, 2016, **79**, 48–54.
114 G. K. Parshetti, F.-H. Lin and R.-A. Doong, *Sens. Actuators, B*, 2013, **186**, 34–43.
115 F. Mo, J. Xie, T. Wu, M. Liu, Y. Zhang and S. Yao, *Food Chem.*, 2019, **292**, 253–259.
116 J. Lu, Y. Hu, P. Wang, P. Liu, Z. Chen and D. Sun, *Sens. Actuators, B*, 2020, **311**, 127909.
117 X. Wei, S. Song, W. Song, W. Xu, L. Jiao, X. Luo, N. Wu, H. Yan, X. Wang, W. Gu, L. Zheng and C. Zhu, *Anal. Chem.*, 2021, **93**, 5334–5342.
118 Y. Niu, K. Kang, B. Wang, L. Wang, C. Li, X. Gao, Z. Zhao and X. Ji, *Talanta*, 2024, **268**, 125349.
119 H. Yu, M. Wang, J. Cao, Y. She, Y. Zhu, J. Ye, J. Wang, S. Lao and A. M. Abd El-Aty, *Anal. Lett.*, 2021, **55**, 427–437.
120 P. Chen, S. Li, C. Jiang, Z. Wang and X. Ma, *Food Biosci.*, 2023, **54**, 102885.
121 S. Wang, Y. Qin and Z. Zou, *Anal. Lett.*, 2015, **49**, 1209–1220.
122 L. Yang, S. J. Zhen, Y. F. Li and C. Z. Huang, *Nanoscale*, 2018, **10**, 11942–11947.
123 L. Zhang, R. Huang, W. Liu, H. Liu, X. Zhou and D. Xing, *Biosens. Bioelectron.*, 2016, **86**, 1–7.
124 Z. Xi, K. Wei, Q. Wang, M. J. Kim, S. Sun, V. Fung and X. Xia, *J. Am. Chem. Soc.*, 2021, **143**, 2660–2664.
125 D. P. Cormode, L. Gao and H. Koo, *Trends Biotechnol.*, 2018, **36**, 15–29.
126 T. Lin, Y. Qin, Y. Huang, R. Yang, L. Hou, F. Ye and S. Zhao, *Chem. Commun.*, 2018, **54**, 1762–1765.
127 Q. Fu, X. Zhou, M. Wang and X. Su, *Anal. Chim. Acta*, 2022, **1216**, 339993.
128 Y. He, B. Xu, W. Li and H. Yu, *J. Agric. Food Chem.*, 2015, **63**, 2930–2934.
129 F. Luo, Y. Lin, L. Zheng, X. Lin and Y. Chi, *ACS Appl. Mater. Interfaces*, 2015, **7**, 11322–11329.
130 H. Chen, T. Yang, F. Liu and W. Li, *Sens. Actuators, B*, 2019, **286**, 401–407.
131 M. Khairy, H. A. Ayoub and C. E. Banks, *Food Chem.*, 2018, **255**, 104–111.
132 J. Feng, Y. Li, M. Li, F. Li, J. Han, Y. Dong, Z. Chen, P. Wang, H. Liu and Q. Wei, *Biosens. Bioelectron.*, 2017, **91**, 441–448.
133 Y. Hu, H. Cheng, X. Zhao, J. Wu, F. Muhammad, S. Lin, J. He, L. Zhou, C. Zhang, Y. Deng, P. Wang, Z. Zhou, S. Nie and H. Wei, *ACS Nano*, 2017, **11**, 5558–5566.
134 J. Li, K. M. Koo, Y. Wang and M. Trau, *Small*, 2019, **13**, 1904689.
135 T. Wu, S. Yu, L. Dai, J. Feng, X. Ren, H. Ma, X. Wang, Q. Wei and H. Ju, *ACS Sens.*, 2022, **7**, 1732–1739.
136 D. Wu, N. Hu, J. Liu, G. Fan, X. Li, J. Sun, C. Dai, Y. Suo, G. Li and Y. Wu, *Talanta*, 2018, **190**, 103–109.
137 Z. Jiang, P. Gao, L. Yang, C. Huang and Y. Li, *Anal. Chem.*, 2015, **87**, 12177–12182.
138 Y. Xuan, Y. Gao, Y. Zhao, W. Zhang, X. Bian, M. Zhang, R. Zhang and S. Zhang, *Sens. Actuators, B*, 2024, **411**, 135692.
139 W. Zou, L. Wang, J. Hao, L. Jiang, W. Du, T. Ying, X. Cai, H. Ran, J. Wu and Y. Zheng, *Composites, Part B*, 2022, **234**, 109707.
140 N. Tao, S. Chen, S. Mahdinloo, Q. Zhang, T. Lan, Q. Saiding, S. Chen, Y. Xiong, W. Tao and J. Ouyang, *Nano Today*, 2024, **57**, 102371.
141 Y. Liu, B. Wang, J. Zhu, X. Xu, B. Zhou and Y. Yang, *Adv. Mater.*, 2023, **35**, 2208512.
142 X. Liu, Z. Liu, K. Dong, S. Wu, Y. Sang, T. Cui, Y. Zhou, J. Ren and X. Qu, *Biomaterials*, 2020, **258**, 120263.
143 C. Cao, N. Yang, Y. Su, Z. Zhang, C. Wang, X. Song, P. Chen, W. Wang and X. Dong, *Adv. Mater.*, 2022, **34**, 2203236.

144 S. Zhong, Z. Zhang, Y. Zhao, S. Wang, Q. Hu and L. Li, *Nanoscale*, 2023, **15**, 16619–16625.
145 C. Qi, W.-H. Wang, J.-F. Zheng, L.-W. Jiang, C. Meng, H. Liu and J.-J. Wang, *J. Mater. Sci.*, 2023, **58**, 5773–5787.
146 W. He, X. Han, H. Jia, J. Cai, Y. Zhou and Z. Zheng, *Sci. Rep.*, 2017, **7**, 7.
147 J. Shen, T. W. Rees, Z. Zhou, S. Yang, L. Ji and H. Chao, *Biomaterials*, 2020, **251**, 120079.
148 S. Zhu, H. Xu, W. Guo, M. Yang, H. Tan, S. Hou, J. Yao, H. Luo, Y. Yao, J. Zhao, Y. Wei, X. Sun and B. Ying, *Adv. Healthcare Mater.*, 2024, 202403002.
149 L. Zeng, Y. Han, Z. Chen, K. Jiang, D. Golberg and Q. Weng, *Adv. Sci.*, 2021, **8**, 2101184.
150 C. Zhang, X. Cheng, M. Chen, J. Sheng, J. Ren, Z. Jiang, J. Cai and Y. Hu, *Colloids Surf., B*, 2017, **160**, 345–354.
151 Y. Song, J. Wang, L. Liu, Q. Sun, Q. You, Y. Cheng, Y. Wang, S. Wang, F. Tan and N. Li, *Mol. Pharm.*, 2018, **15**, 1941–1953.
152 J. Liu, J. Zhang, F. Huang, Y. Deng, B. Li, R. Ouyang, Y. Miao, Y. Sun and Y. Li, *Acta Biomater.*, 2020, **113**, 570–583.
153 Z. Zhou, J. Xie, S. Ma, X. Luo, J. Liu, S. Wang, Y. Chen, J. Yan and F. Luo, *ACS Omega*, 2021, **6**, 10723–10734.
154 S. Zhang, Z. Yang, J. Hao, F. Ding, Z. Li and X. Ren, *Chem. Eng. J.*, 2022, **432**, 134309.
155 J. Cao, Q. Sun, A.-G. Shen, B. Fan and J.-M. Hu, *Chem. Eng. J.*, 2021, **422**, 130090.
156 T. Yao, X. Zeng, H. Li, T. Luo, X. Tao and H. Xu, *Int. J. Biol. Macromol.*, 2024, **269**, 132115.
157 W. Wang, Y. Cui, X. Wei, Y. Zang, X. Chen, L. Cheng and X. Wang, *ACS Nano*, 2024, **18**, 15845–15863.
158 J. Guo, W. Wei, Y. Zhao and H. Dai, *Regen. Biomater.*, 2022, **9**, rbac041.
159 T. Wang, D. Dong, T. Chen, J. Zhu, S. Wang, W. Wen, X. Zhang, H. Tang, J. Liang, S. Wang and H. Xiong, *Chem. Eng. J.*, 2022, **446**, 137142.
160 Y. Feng, J. Qin, Y. Zhou, Q. Yue and J. Wei, *J. Colloid Interface Sci.*, 2022, **606**, 826–836.
161 Y. Liu, B. Wang, J. Zhu, X. Xu, B. Zhou and Y. Yang, *Adv. Mater.*, 2023, **35**, 2208512.
162 Y. Liu, B. Xu, M. Lu, S. Li, J. Guo, F. Chen, X. Xiong, Z. Yin, H. Liu and D. Zhou, *Bioact. Mater.*, 2022, **12**, 246–256.
163 H. Geng, X. Li, X. J. Gao, Y. Cong, Q. Liu, J. Li, Y. Guan, L. Wang and W. He, *Nano Today*, 2023, **52**, 101989.
164 X. Wang, Q. Shi, Z. Zha, D. Zhu, L. Zheng, L. Shi, X. Wei, L. Lian, K. Wu and L. Cheng, *Bioact. Mater.*, 2021, **6**, 4389–4401.
165 M. M. Pan, Y. Ouyang, Y. L. Song, L. Q. Si, M. Jiang, X. Yu, L. Xu and I. Willner, *Small*, 2022, **18**, e2200548.
166 Y. Fan, X. Gan, H. Zhao, Z. Zeng, W. You and X. Quan, *Chem. Eng. J.*, 2022, **427**, 131572.
167 X. Wang, Q. Shi, Z. Zha, D. Zhu, L. Zheng, L. Shi, X. Wei, L. Lian, K. Wu and L. Cheng, *Bioact. Mater.*, 2021, **6**, 4389–4401.
168 Y. Liu, F. Yang, P. Liu, C. Lou, L. Zhu and Y. Yang, *ACS Appl. Nano Mater.*, 2024, **7**, 23076–23086.
169 D. Wang, B. Zhang, H. Ding, D. Liu, J. Xiang, X. J. Gao, X. Chen, Z. Li, L. Yang, H. Duan, J. Zheng, Z. Liu, B. Jiang, Y. Liu, N. Xie, H. Zhang, X. Yan, K. Fan and G. Nie, *Nano Today*, 2021, **40**, 101243.
170 T. Qin, R. Ma, Y. Yin, X. Miao, S. Chen, K. Fan, J. Xi, Q. Liu, Y. Gu, Y. Yin, J. Hu, X. Liu, D. Peng and L. Gao, *Theranostics*, 2019, **9**, 6920–6935.

